# NAVAL POSTGRADUATE SCHOOL

## MONTEREY, CALIFORNIA

# THESIS

**EMULATION OF WIND POWER WITH A DC MACHINE TO PROVIDE INPUT TO A DOUBLY-FED INDUCTION MACHINE**

by

Jonathan T. Hines

March 2012

| Thesis Advisors: | Alexander L. Julian |
| | Giovanna Oriti |

**Approved for public release; distribution is unlimited**

THIS PAGE INTENTIONALLY LEFT BLANK

| REPORT DOCUMENTATION PAGE | | *Form Approved OMB No. 0704-0188* |
|---|---|---|
| Public reporting burden for this collection of information is estimated to average 1 hour per response, including the time for reviewing instruction, searching existing data sources, gathering and maintaining the data needed, and completing and reviewing the collection of information. Send comments regarding this burden estimate or any other aspect of this collection of information, including suggestions for reducing this burden, to Washington headquarters Services, Directorate for Information Operations and Reports, 1215 Jefferson Davis Highway, Suite 1204, Arlington, VA 22202-4302, and to the Office of Management and Budget, Paperwork Reduction Project (0704-0188) Washington DC 20503. | | |
| **1. AGENCY USE ONLY** *(Leave blank)* | **2. REPORT DATE** March 2012 | **3. REPORT TYPE AND DATES COVERED** Master's Thesis |
| **4. TITLE AND SUBTITLE** Emulation of Wind Power with a DC Machine to Provide Input to a Doubly-Fed Induction Machine | | **5. FUNDING NUMBERS** |
| **6. AUTHOR(S)** Jonathan T. Hines | | |
| **7. PERFORMING ORGANIZATION NAME(S) AND ADDRESS(ES)** Naval Postgraduate School Monterey, CA 93943-5000 | | **8. PERFORMING ORGANIZATION REPORT NUMBER** |
| **9. SPONSORING /MONITORING AGENCY NAME(S) AND ADDRESS(ES)** N/A | | **10. SPONSORING/MONITORING AGENCY REPORT NUMBER** |
| **11. SUPPLEMENTARY NOTES** The views expressed in this thesis are those of the author and do not reflect the official policy or position of the Department of Defense or the U.S. Government. IRB Protocol number _____N/A_____. | | |
| **12a. DISTRIBUTION / AVAILABILITY STATEMENT** Approved for public release; distribution is unlimited | | **12b. DISTRIBUTION CODE** A |

**13. ABSTRACT (maximum 200 words)**

The behavioral modeling of a separately excited direct current (DC) motor as a prime mover for a doubly-fed induction machine (DFIM) is studied in this thesis. The output torque of the DC motor is computed in the simulation under controlled parameters. The input to the DFIM, used as a doubly-fed induction generator (DFIG), is taken from the DC motor. In theory, the combination of the two machines can be used to emulate various wind patterns and their expected electrical returns for a given DFIM-based wind turbine.

A Simulink model was created to appropriately emulate the operation of the DC machine. That model was then incorporated into an existing model of a DFIM. The resulting simulations are compared to system operating data to determine if machine speed is being correctly modeled. The speeds determined by the simulator accurately track those that are gathered from lab data.

Operating speeds of the system were mapped to historical wind speeds in a geographical area. Output power of the DC motor for the different operating speeds was calculated and plotted. The data confirmed the theory of the proportionality of the rotational output power of a DC motor.

| **14. SUBJECT TERMS** Direct Current (DC) Motor, Doubly-fed induction machine (DFIM), Doubly-fed induction generator (DFIG),  Wind Power, Simulink Model | | **15. NUMBER OF PAGES** 91 |
|---|---|---|
| | | **16. PRICE CODE** |
| **17. SECURITY CLASSIFICATION OF REPORT** Unclassified | **18. SECURITY CLASSIFICATION OF THIS PAGE** Unclassified | **19. SECURITY CLASSIFICATION OF ABSTRACT** Unclassified | **20. LIMITATION OF ABSTRACT** UU |

THIS PAGE INTENTIONALLY LEFT BLANK

**EMULATION OF WIND POWER WITH A DC MACHINE TO PROVIDE INPUT TO A DOUBLY-FED INDUCTION MACHINE**

Jonathan T. Hines
Lieutenant, United States Navy
B.S., Auburn University, 2005

Submitted in partial fulfillment of the
requirements for the degree of

**MASTER OF SCIENCE IN ELECTRICAL ENGINEERING**

from the

**NAVAL POSTGRADUATE SCHOOL**
**March 2012**

Author:                 Jonathan T. Hines

Approved by:       Alexander L. Julian
                       Thesis Advisor

                       Giovanna Oriti
                       Thesis Advisor

                       R. Clark Robertson
                       Chair, Department of Electrical and Computer Engineering

THIS PAGE INTENTIONALLY LEFT BLANK

# ABSTRACT

The behavioral modeling of a separately excited direct current (DC) motor as a prime mover for a doubly-fed induction machine (DFIM) is studied in this thesis. The output torque of the DC motor is computed in the simulation under controlled parameters. The input to the DFIM, used as a doubly-fed induction generator (DFIG), is taken from the DC motor. In theory, the combination of the two machines can be used to emulate various wind patterns and their expected electrical returns for a given DFIM-based wind turbine.

A Simulink model was created to appropriately emulate the operation of the DC machine. That model was then incorporated into an existing model of a DFIM. The resulting simulations are compared to system operating data to determine if machine speed is being correctly modeled. The speeds determined by the simulator accurately track those that are gathered from lab data.

Operating speeds of the system were mapped to historical wind speeds in a geographical area. Output power of the DC motor for the different operating speeds was calculated and plotted. The data confirmed the theory of the proportionality of the rotational output power of a DC motor.

THIS PAGE INTENTIONALLY LEFT BLANK

# TABLE OF CONTENTS

# LIST OF FIGURES

# LIST OF TABLES

THIS PAGE INTENTIONALLY LEFT BLANK

# LIST OF ACRONYMS AND ABBREVIATIONS

| | |
|---|---|
| A | Amperes |
| DC | Direct Current |
| DFIG | Doubly Fed Induction Generator |
| H | Henries |
| $i_a$ | Armature Current |
| $i_f$ | Field Current |
| $L_{AA}$ | Armature Self Inductance |
| $L_{AF}$ | Mutual Inductance Between Armature and Field |
| $L_{FF}$ | Field Self Inductance |
| $P_{i^2 r}$ | Armature Losses |
| $P_{in}$ | DC Machine Rotor Input Power |
| $P_{out}$ | DC Machine Rotational Output Power |
| $r_a$ | Armature Resistance |
| $r_f$ | Field Resistance |
| RPM | Revolutions Per Minute |
| $RPM_O$ | Motor Operation Speed Scaled to Wind Speed |
| $T_e$ | Output Torque of DC Machine |
| V | Volts |
| $v_a$ | Armature Voltage Supplied to DC Motor |
| $v_{a,source}$ | Source Armature Voltage |

$v_f$        Field Voltage Supplied to DC Motor

$v_{f,source}$        Source Field Voltage

$\omega_r$        Rotational Speed

# EXECUTIVE SUMMARY

The theory of the separately excited direct current (DC) motor as a means to create a simulated model of the machine is explored in this thesis. This model is used as an input to a doubly-fed induction generator (DFIG) model. The model is expected to provide a more accurate evaluation of system behavior than was previously utilized in earlier research on this system because the earlier research did not include a detailed model of a DC machine as is the case in the lab hardware.

The separately excited DC motor was investigated to develop the equations necessary to produce the model. Once the required equations were understood, the model was designed using the Simulink program. This model of the DC motor was incorporated within a larger simulation of a DFIG system with the DC motor acting as the prime mover.

Test runs were completed in the lab using the operational setup. Speed runs were conducted with commanded speed beginning at 1,441 revolutions per minute (RPM) and then shifting to 1,981 RPM. The data from these runs was output to a file that could be incorporated into Matlab.

Next, the simulation of the overall DFIG system was run using the same commanded speed changes. A plot was constructed of the operational speed of the simulation versus time. The model was tested for validity by collecting data from lab experimentation and then comparing the data to the output of the model. The resulting speed testing plot comparing measured and simulated data is shown in Figure 1.
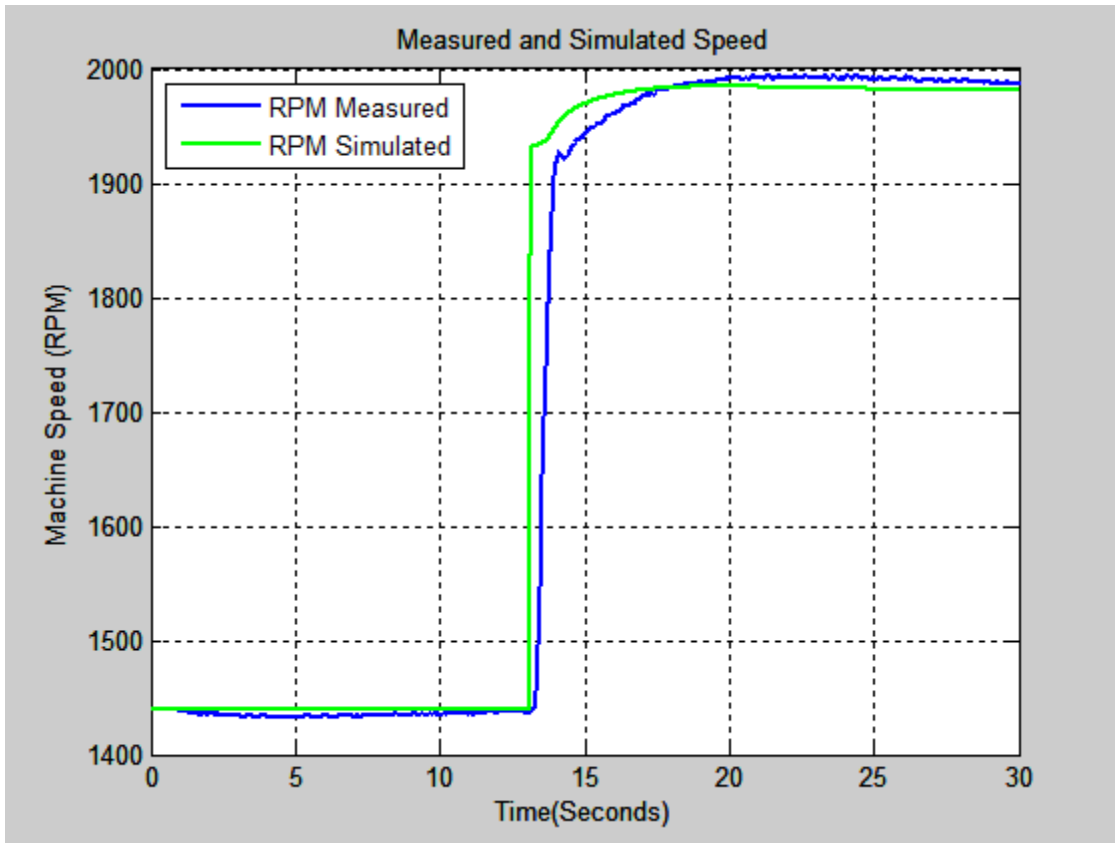
Figure 1.          Measured and simulated system RPM vs. time.

The comparison of simulated speed and the measured speed of the system is shown in Figure 1. The simulation results and the results obtained from the operational data for the experimental run for speed are closely matched.

The power data was also gathered from the operational runs. The armature input power from the DC motor model and that of the actual machine are shown in Figure 2. The steady state values of the Simulink analysis closely approximate those from the machine run. The machine model does not contain enough detail to fully simulate the drop in power at the transition in speed, but the dip in the simulated power is similar to that observed in the measurements.
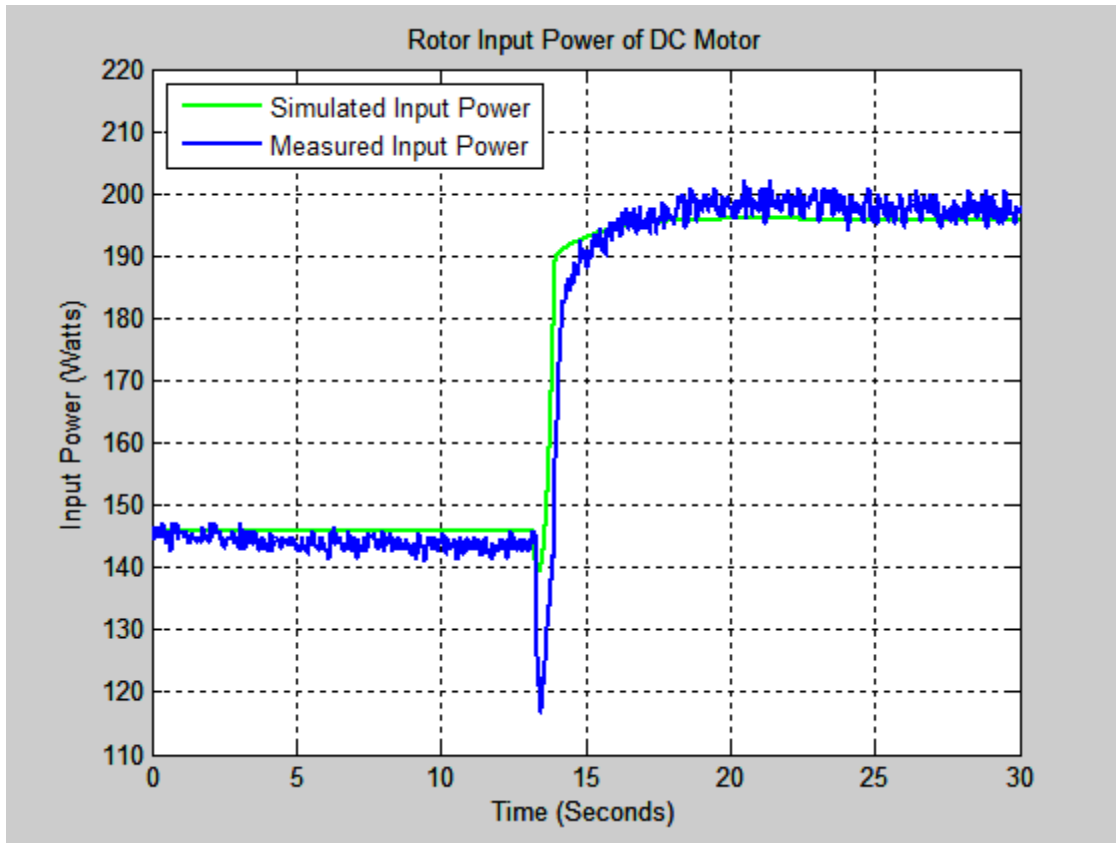
Figure 2.        Measured and simulated input power vs. time.

Next, the average monthly wind speeds for a particular area were scaled to operational rotational speeds of the DC motor. The output power was computed using the simulated model. The correlation between the operational speed of the DC motor and the output power was confirmed. The plots of the scaled speed and the corresponding output power are shown in Figures 3 and 4, respectively. Each plot begins with the values for January at the left and shifts months every four seconds. The conversion of the wind speed to a particular power level depends on the design of the turbine/gearbox/generator, and no specific hardware is being represented in this thesis.
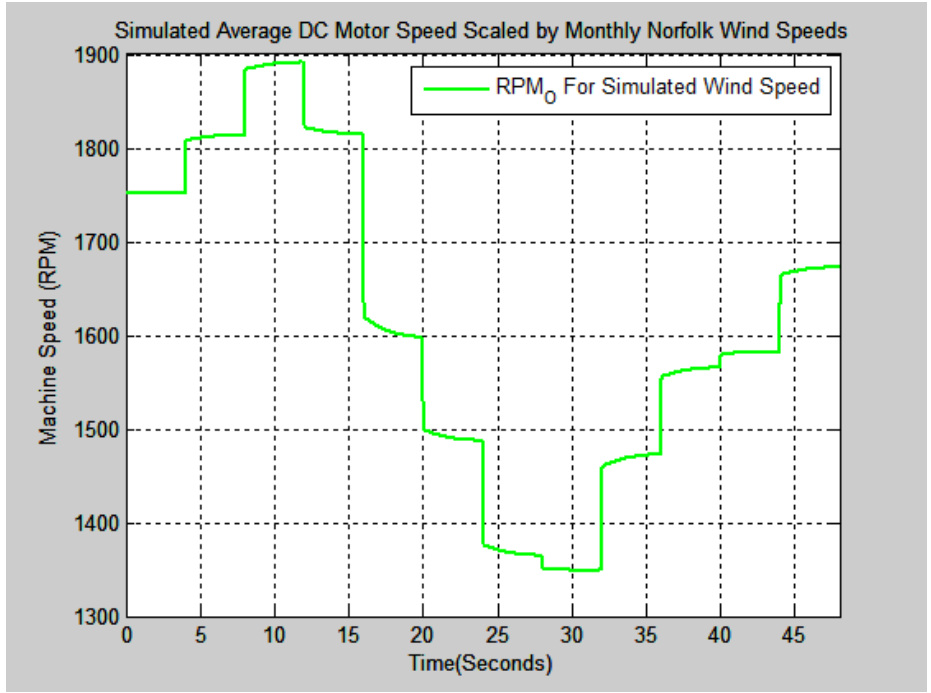
Figure 3.        Simulated average DC motor speed by month for wind turbine in Norfolk.
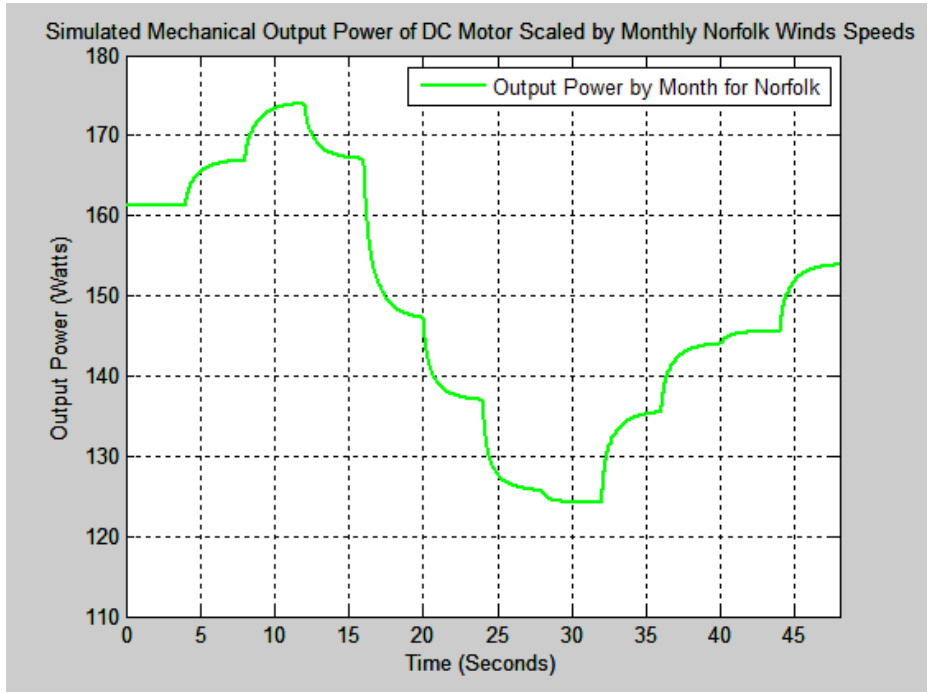


Figure 4.        Simulated average DC motor output power by month for Norfolk.

In summary, a model of the separately excited DC motor was created using Simulink. The motor model responded predictably and accurately to changes in speed. The input power also responded accordingly leading to a predictable output power of the system. This will allow for future research to build upon the model to perform further analysis of the DFIG system at the Naval Postgraduate School.

THIS PAGE INTENTIONALLY LEFT BLANK

# ACKNOWLEDGMENTS

First and foremost, I thank God for the perseverance to see this thesis through. If not for His grace and mercy, I would have never been able to complete the task.

Thank you to all of the staff and faculty of the Naval Postgraduate School who have facilitated the wonderful educational opportunity that I have had here. The dedication and time of so many have contributed to my tour being such a wonderful time for professional and personal growth. In particular, I want to thank Professor Julian for his advice and knowledge during this process. I learned so much from you and you have my deepest gratitude.

Finally, I must thank the three most important people in my life. To my beautiful wife, Linda, you are my rock and my support. Without your love and encouragement, along with your calming presence, I never would have survived the stresses of the last two years. I am so blessed to have you. To my wonderful sons, Jonathan and Joshua, thank you so much for your boundless enthusiasm and joy. You two could always make me laugh and you never failed at helping me put things in perspective. Whenever I felt down, you helped me to realize that things were never really bad as long as I had the love of you guys and your mother.

THIS PAGE INTENTIONALLY LEFT BLANK

# I.   INTRODUCTION AND BACKGROUND INFORMATION

## A.   BACKGROUND

Per the Energy Policy Act of 2005, the United States government is requiring that federal agencies, including the Department of Defense (DoD), actively increase their usage of renewable energy sources. By the year 2025, the DoD is required to produce or procure at least 25% of its total facility energy from these sources [1]. Meeting this goal requires an investment in various forms of technology to produce and implement renewable sources.

Wind power is a potential source of energy that the DoD should exploit. This would be of great help in achieving the goals of The Energy Policy Act. Wind technology can provide a proven method of renewable energy.

Doubly-fed induction generators (DFIG) are often used in wind power generation to supply power to a grid [2]. The turbine blades are connected to a gearbox that provides input torque to a DFIG. A typical DFIG system is shown in Figure 5.
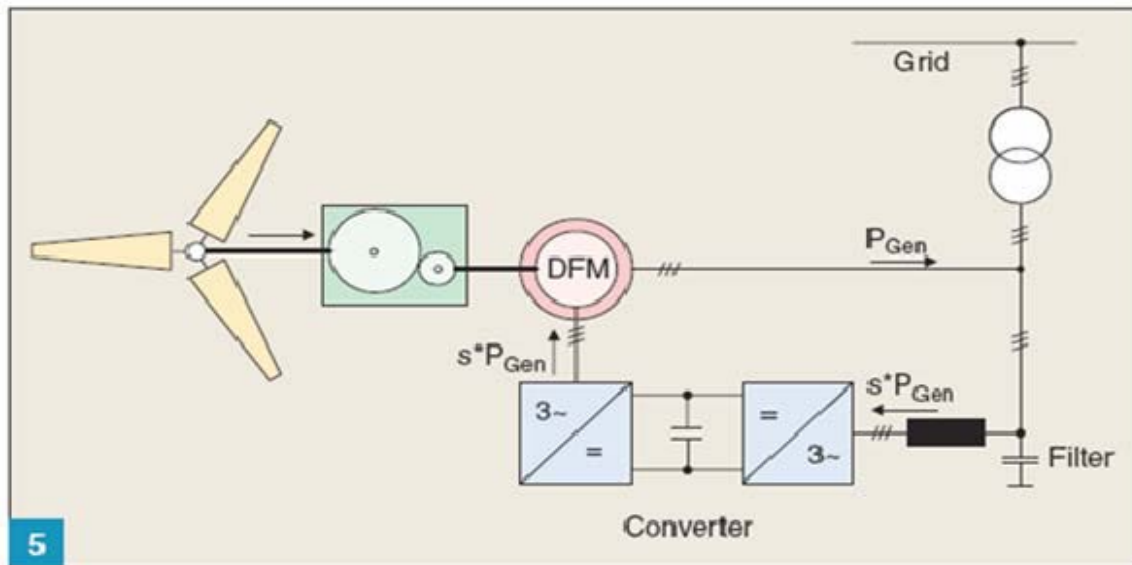


Figure 5.    DFIG connected to wind turbine, from [2].

The Naval Postgraduate School has developed a wind power emulator that replaces the turbine and associated gearbox with a direct current (DC) motor. A simulation was created with this project to predict and explain its operation [3]. This setup is displayed in Figure 6.
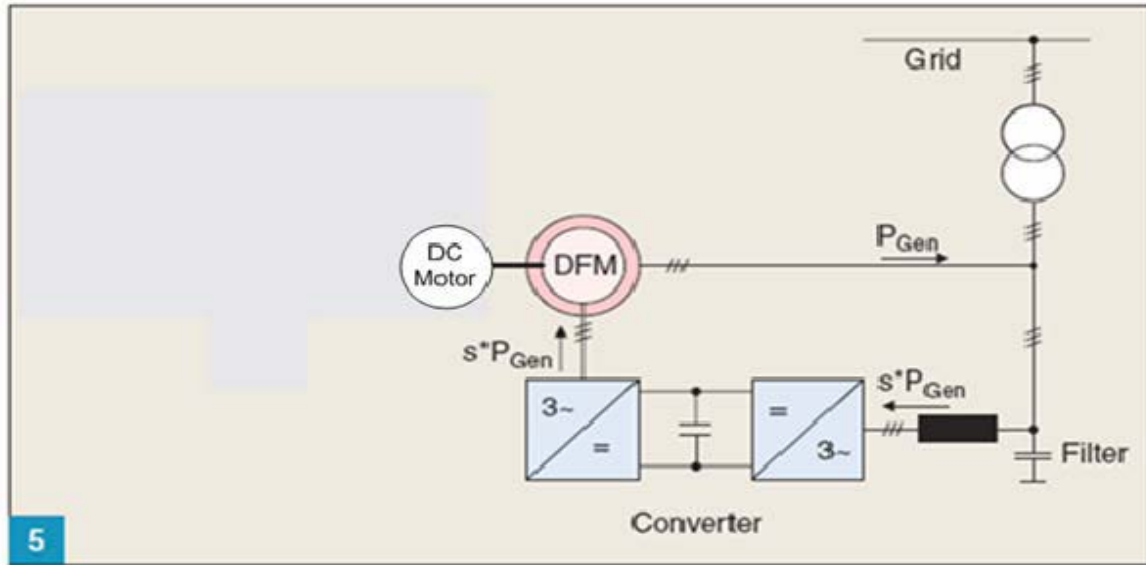


Figure 6.     DFIG connected to DC motor, from [4].

B.     OBJECTIVE

The objective of this thesis is to provide better predictions of the operational speed and input torque of the machines through modeling of the DC machine. The initial simulations in Matlab used a torque constant as input into the modeled DFIG [2]. While this method is more than sufficient for studies of the electrical output of the DFIG itself, it does not accurately predict the torque of the DC machine, particularly when transitioning between different speeds. The hypothesis is that creating a full model of a DC machine using Matlab and Simulink and providing input to the Simulink model of the DFIG will provide a greater level of predictability of system behavior.

Verifying the relationship between output power and speed was a secondary goal of the study.   Theoretically, the DC motor can be used to model the output power and

2

torque provided by turbine blading and the gearbox [2]. The goal is to model the rotational output power through the use of Simulink and prove the interconnection between power and speed.

## C.     APPROACH

The first step in this thesis was to understand the operation of the DC machine that was to be used. The machine in question was a separately-excited DC motor. By leveraging previous studies, a mathematical model of the DC motor was created. References [4], [5], [6], and [7] were used to gather this information. Next, the model of the separately-excited DC motor was created using Simulink. The model of the DC motor was then implemented as a replacement for the constant torque input in the DFIG Simulink model [2]. Machine speed data, including a change in operating speed, and output power data were obtained from equipment operation in the lab. This data was compared to the predicted speed and predicted output power from the simulation to validate the simulation accuracy.

## D.     THESIS ORGANIZATION

The theory of operation for the separately excited DC motor is covered in Chapter II. The equations for the field and armature voltages and currents, torque, and power are presented. The Lab-Volt 8211 DC Motor/Generator is employed, as part of an operating DFIG system, to provide output data for later analysis. A representative model of the Lab-Volt DC motor is created in Simulink as part of an overall DFIG system [2]. The output data of the model is compared to the actual output of the motor to determine accuracy of the simulation.

A wind profile from a particular geographic area is discussed in Chapter III. The wind speeds of this profile are mapped to motor operating speeds for the simulated DC machine. The output power of the machine is computed by the simulation based on the different speeds of operation.

Conclusions are drawn about the testing results in Chapter IV. The validity of the created model for simulations of the DFIG system is reviewed. Some possibilities for future work to build upon this topic are also presented.

## II. SIMULATED DC MACHINE ANALYSIS

### A. INTRODUCTION

The equations that define a DC motor are reviewed in this section [5]. Using values determined from previous research on this machine, we created a model using Matlab's Simulink software. The model, used as the prime mover for the DFIG simulation, is evaluated using a specific operational profile. The speed output is compared to the output of the actual machinery running the same profile to test the validity of the model.

### B. DC MOTOR EQUATIONS

#### 1. Basic DC Motor Theory

DC motors have been used for many years, and the characteristics of these machines are well understood. The overall principle behind the operation is quite simple. A current-carrying conductor, in the presence of a magnetic field, experiences a force that is perpendicular to both the current and the direction of the magnetic field. Using this knowledge to produce a practical DC motor is difficult.

Figure 7 is a representation of a simple DC machine [5]. The stator poles are wound with field windings, while the rotor has its own coil. A commutator, made up of two semicircular copper segments, is mounted at the end of the rotor. The terminals of the rotor coil are connected to the copper segment. Voltage is supplied to the rotor from a stationary circuit via carbon brushes, which causes a current to flow through the rotor coils. The commutator allows for current to be supplied in a consistent direction so that the application of electrical torque on the rotor forces rotation in the same direction at all times [5].
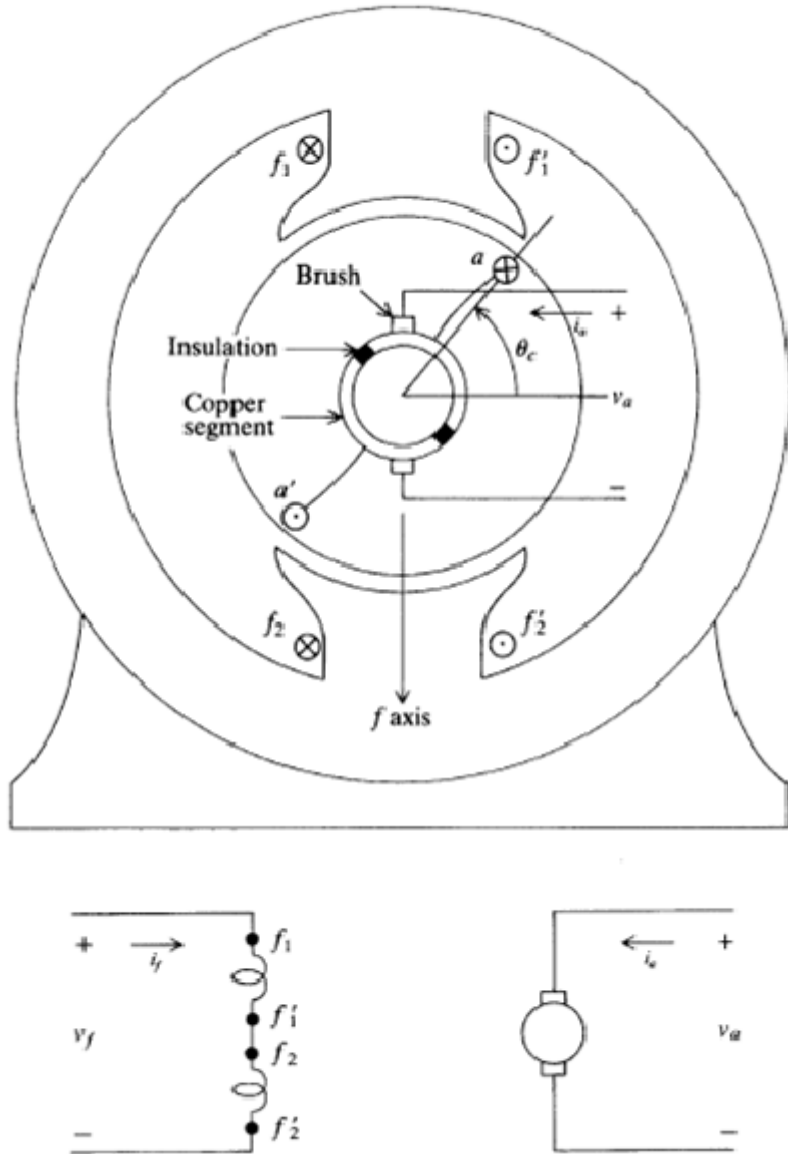
Figure 7.     Elementary 2-pole DC machine, from [5].

The commutating action causes the rotor coils to appear as a stationary winding with respect to the field. The magnetic axis of the rotor windings always appears perpendicular to that of the stator windings. Because of this, there is no induction of voltages in one winding due to a time rate of change of current in the other [5].

The equations are derived in [5] to generate an equation matrix in the form of

Equation Chapter 2 Section 1

$$\begin{bmatrix} v_f \\ v_a \end{bmatrix} = \begin{bmatrix} r_f + \dfrac{d}{dt}L_{FF} & 0 \\ \omega_r L_{AF} & r_a + \dfrac{d}{dt}L_{AA} \end{bmatrix} \begin{bmatrix} i_f \\ i_a \end{bmatrix}, \tag{2.1}$$

where $v_f$ and $v_a$ are the field and the armature voltages, respectively, $r_f$ and $r_a$ are the field and armature resistances, respectively, and $i_f$ and $i_a$ are the field and armature currents, respectively. Rotor speed is $\omega_r$. The self-inductance of the armature and the field windings are represented by $L_{AA}$ and $L_{FF}$, respectively. The mutual inductance between the armature windings and the field windings is represented by $L_{AF}$. From [5], the electric torque $T_e$ is calculated through the mutual inductance of the motor and the armature and field currents as

$$T_e = L_{AF} i_f i_a. \tag{2.2}$$

Equation (2.2) is used to compute the torque that is supplied to the DFIG system through the Simulink program.

### 2.    DC Motor Equations for Separately-Excited Windings

The DC motor used for the purposes of this study had separate winding excitation. This simply means that a field rheostat is located in the field circuit allowing for adjustment of the field current. Figure 8, from [5], shows an equivalent separately excited DC motor circuit with the field rheostat designated as $r_x$.
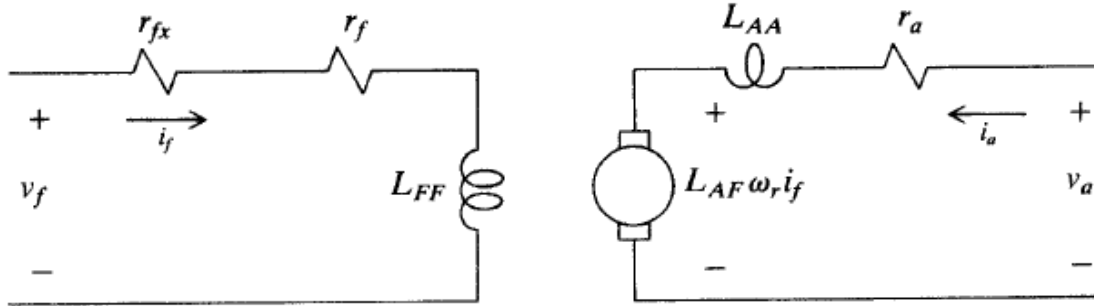
Figure 8.    Equivalent circuit for separately excited DC machine, from [5].

The value of the field rheostat resistance must be taken into account when performing calculations to determine motor operating characteristics.

## C.    OVERVIEW OF EQUIPMENT CONFIGURATION

A representation of the physical system setup is shown in Figure 9. The specifications of the Lab-Volt motor used for this study are found in Appendix A. The rotor of the DC motor is connected to the rotor of the DFIG to provide input torque for the system.

The field programmable gate array (FPGA) is configured to receive various data from the operating machinery. The output of data is relayed from the machinery to the controlling personal computer via a universal serial bus connection. The data can be retrieved and analyzed further at a later time.

An oscilloscope is connected to provide data analysis during the lab experimentation. It is used to measure the various voltages and currents of interest for the DFIG. The oscilloscope is also used to export data from the operational experiments.

Figure 9.        Equipment setup in lab, from [3]

## D.    SIMULINK MODEL

Equations 2.1 and 2.2 were used to create the model of the DC machine in Simulink. Measurements were taken with a multimeter to determine the field resistance for the DFIG system. The measured and calculated values for armature resistance and mutual inductance were taken from [4]. Rotor speed was initially commanded to 1,440 revolutions per minute (RPM) and then increased to 1,980 RPM. No method was readily available to test for armature and field self-inductance values. Instead, a nominal value is assumed for both the armature and field self-inductance based on information from [5]. The values used throughout the simulation process are shown in Table 1.

9

Table 1.     Values for variables used in DC motor model.

| Values for Simulation Variables | |
|---|---|
| $v_{f,source}$ | 170 V |
| $v_{a,source}$ | 170 V |
| $r_f$ | 6.4 Ω |
| $r_a$ | 8.5 Ω |
| $\omega_r$ | Varied between 151 and 207 radians/second |
| $L_{FF}$ | 30 H |
| $L_{AA}$ | Initially 180H; reduced to 30 H |
| $L_{AF}$ | Initially 3 H, reduced to 2.25 H |
| $i_{f,ref}$ | 0.3125 A |
| $i_{a,ref}$ | 1.25 A |

The next step in the process was to build the Simulink model of the DC motor. The equations for field voltage and armature voltage were obtained from (2.1), to get

$$v_f = r_f i_f + L_{FF} \frac{di_f}{dt} \qquad (2.3)$$

and

$$v_a = \omega_r L_{AF} i_f + r_a i_a + L_{AA} \frac{di_a}{dt}. \qquad (2.4)$$

The field voltage and armature voltage equations were then rearranged to solve for the field current and the armature current, respectively, to yield

$$i_f = \frac{1}{L_{FF}} \int (v_f - r_f i_f) dt \qquad (2.5)$$

and

$$i_a = \frac{1}{L_{AA}} \int (v_a - \omega_r L_{AF} i_f - r_a i_a) dt. \qquad (2.6)$$

Next, Simulink was used to model the motor based on (2.5) and (2.6). Once the separate equations were assembled, the interconnected functions were joined to create a model of a separately-excited DC machine. The torque equation was also produced using

10

connections to the mutual inductance, field current, and armature current. The overall model for the DC motor is shown in Figure 10.
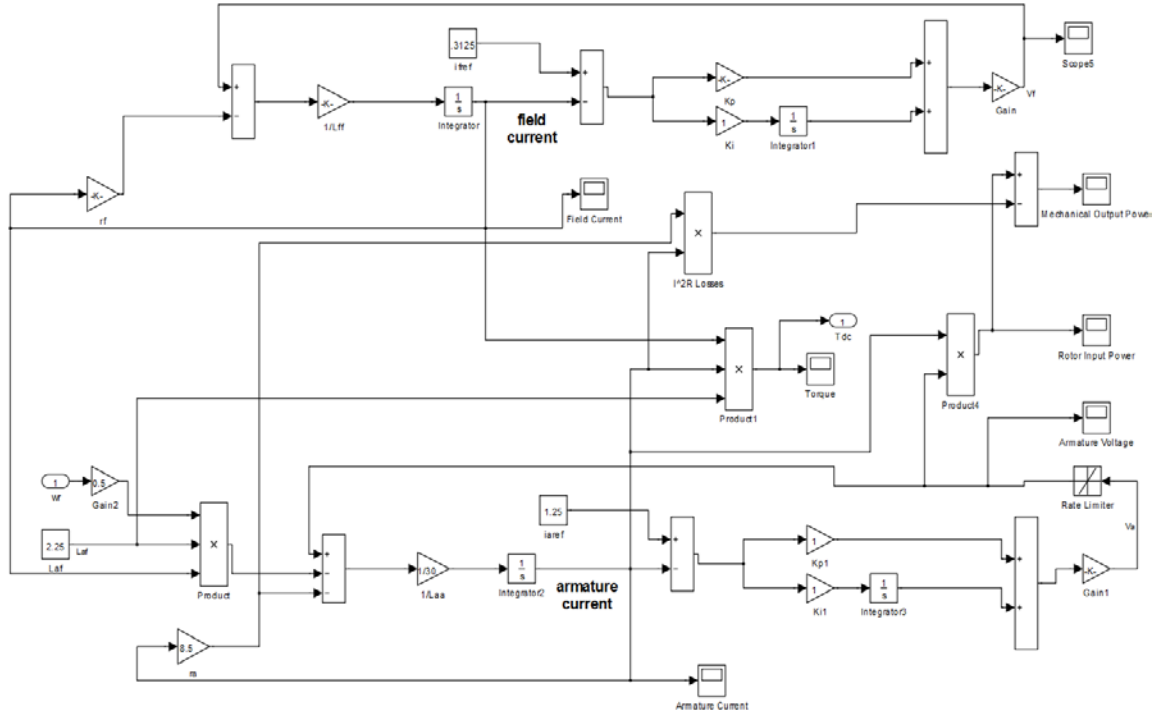


Figure 10.          DC motor model in Simulink.

The field current circuit is located in the upper part of Figure 10. The field current is sent into an amplifier representing field resistance. The value of that product is sent to a negative node on a summing junction where it is added to the field voltage. The output of this summing junction is multiplied by the reciprocal of the self-inductance of the field and subsequently integrated to generate the field current value. Field current is then fed into a proportional integral controller with both values for the gains set to one. The reference field current is set to 0.3125 A in accordance with the DFIG system. The output of the controller is supplied through an amplifier representing the nominal voltage setpoint of 170 V for the field voltage.

11

The armature current was designed in a manner similar to the field current circuit and is located in the lower section of Figure 10. The product junction multiplies the field current, the mutual inductance, and the rotor speed. That output is, in turn, subtracted from the value of the armature voltage. The product of the armature resistance and the armature current is also subtracted from armature voltage at the first summation junction. The armature voltage is rate limited in order to prevent instantaneous changes in voltage. This allows for more a more accurate behavioral model of rotor input power by allowing for a delay reduction in power during the transient. The remainder of the circuit is identical to the field current circuit with the exception of the value for the reference armature current (1.25 A).

The machine output torque is calculated at the center of Figure 10 in accordance with (2.2). The torque is defined as the variable $T_{dc}$ for the drawing.

The calculation for the armature electrical input power is located on the right edge of Figure 10. The formula [5]

$$P_{in} = v_a i_a \tag{2.7}$$

is used to determine the input power into the rotor of the DC motor, where $P_{in}$ is electrical input power to the DC motor armature. The armature losses are found from [5]

$$P_{i^2r} = r_a i_a^{\;2} \tag{2.8}$$

where $P_{i^2r}$ is defined as the armature losses. The armature losses are computed on Figure 10 near the center of the diagram. Next, $P_{i^2r}$ is subtracted from $P_{in}$ to compute a more realistic value for the machine output power that takes into account armature losses for the DC motor. The resulting equation is

$$P_{out} = P_{in} - P_{i^2r} \,, \tag{2.9}$$

where $P_{out}$ is the final computed mechanical output power for the simulation.

## E.    MODEL VALIDATION FOR ARMATURE AND FIELD CURRENTS

The armature and field currents were extracted as data from the operating machinery. The measured values were then compared to the simulated values for accuracy. This step was done to ensure that the simulation was commanding and outputting the values expected before continuing on to more complex calculations. Figure 11 is a plot of the measured and simulated armature and field currents during a transition between 1,441 RPM and 1,981 RPM.
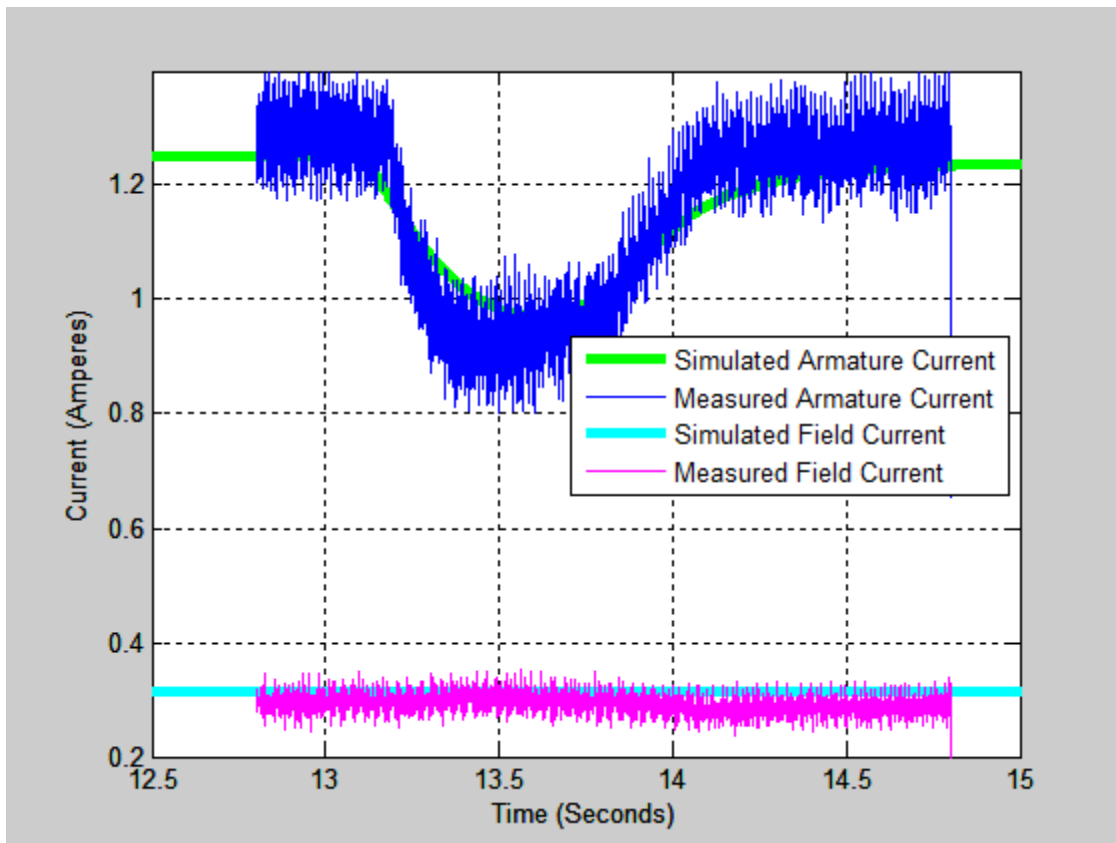


Figure 11.        Measured and simulated armature and field currents.

The values of both simulated currents correspond well with the operational data. The computation of armature current and field current was found to be accurate. Parameters such as input power and machine speed were simulated with the understanding that the currents were correctly modeled.

13

**F. MODEL VALIDATION FOR SPEED**

**1. Comparison between Operational Data and Simulated Data**

In order to validate the accuracy of the circuit model constructed in Simulink, data from the DFIG system in the lab was taken. The system was operated using a specific speed profile. The speed data was extracted from the system and subsequently implemented into the Matlab code for the DFIG system [2] found in Appendix B. This operational speed data was plotted for future comparison as seen in Figure 12.
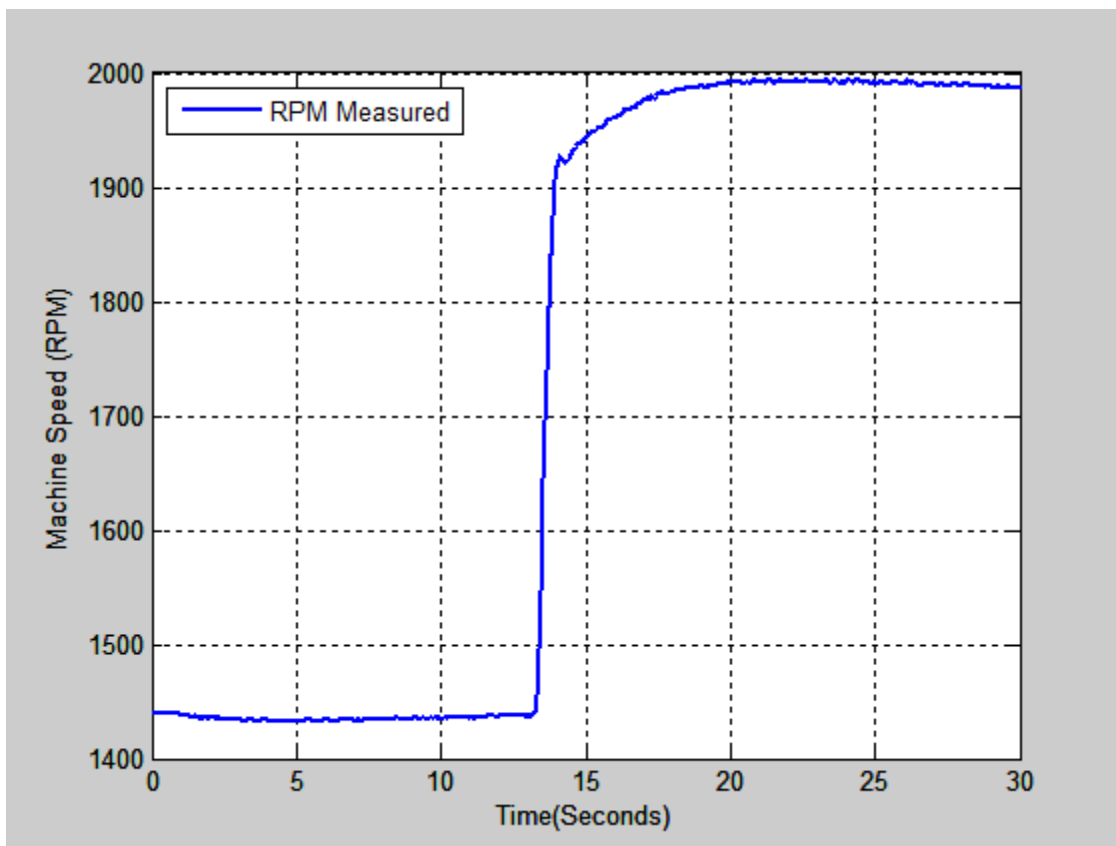


Figure 12.      Measured system RPM vs. time.

The system is initially commanded to operate at a speed of 1,441 RPM. Thirteen seconds later, the requested speed is raised. The DFIG system settles at a new speed of 1,981 RPM.

The simulation was adjusted to reflect the magnitude and duration of the speeds in the operational portion. The torque constant was removed from the simulation, and the input torque to the DFIG was connected to the output of the DC motor model. The overall model of the DFIG system, including the separately excited DC motor, is shown in Appendix C. The simulation was executed and speed data was collected and plotted. The plot of the simulated speed data for the test runs is displayed in Figure 13.
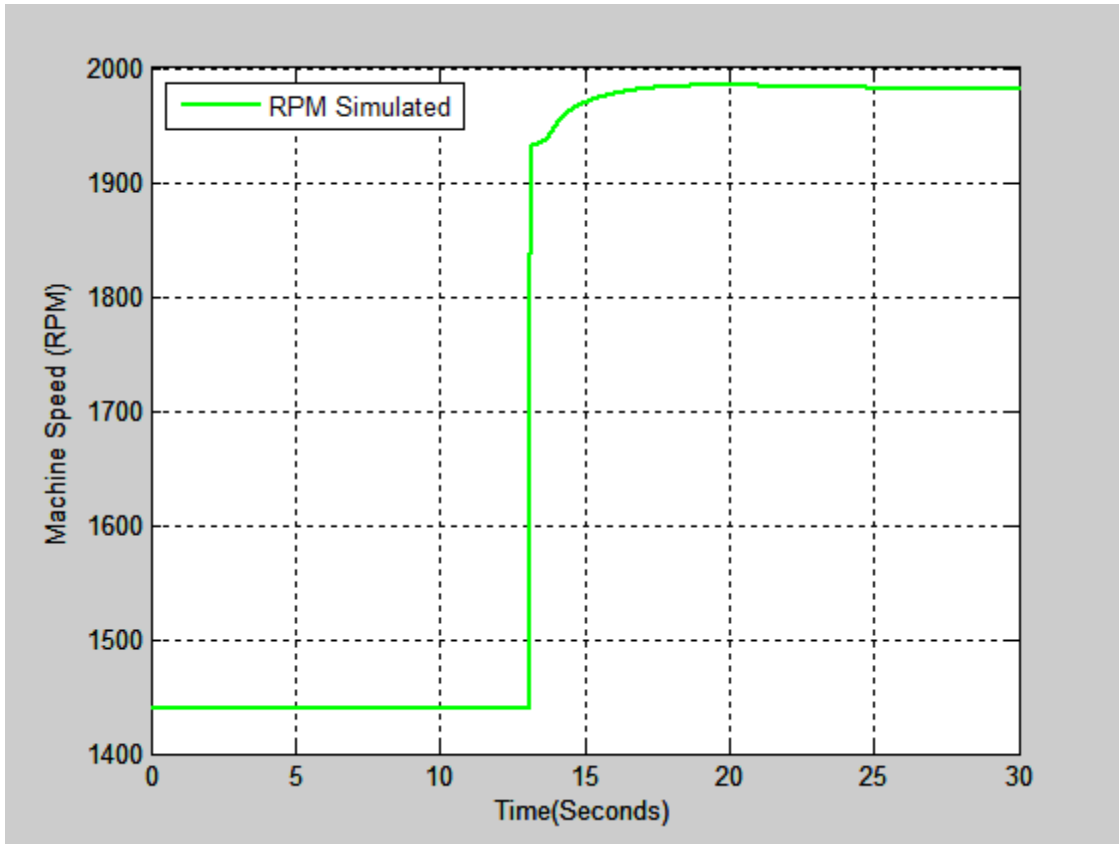


Figure 13.        Simulated system RPM vs. time.

15

The measured data and the simulated data were plotted together on the same graph to provide for easier analysis. This yielded the data pictured in Figure 14.
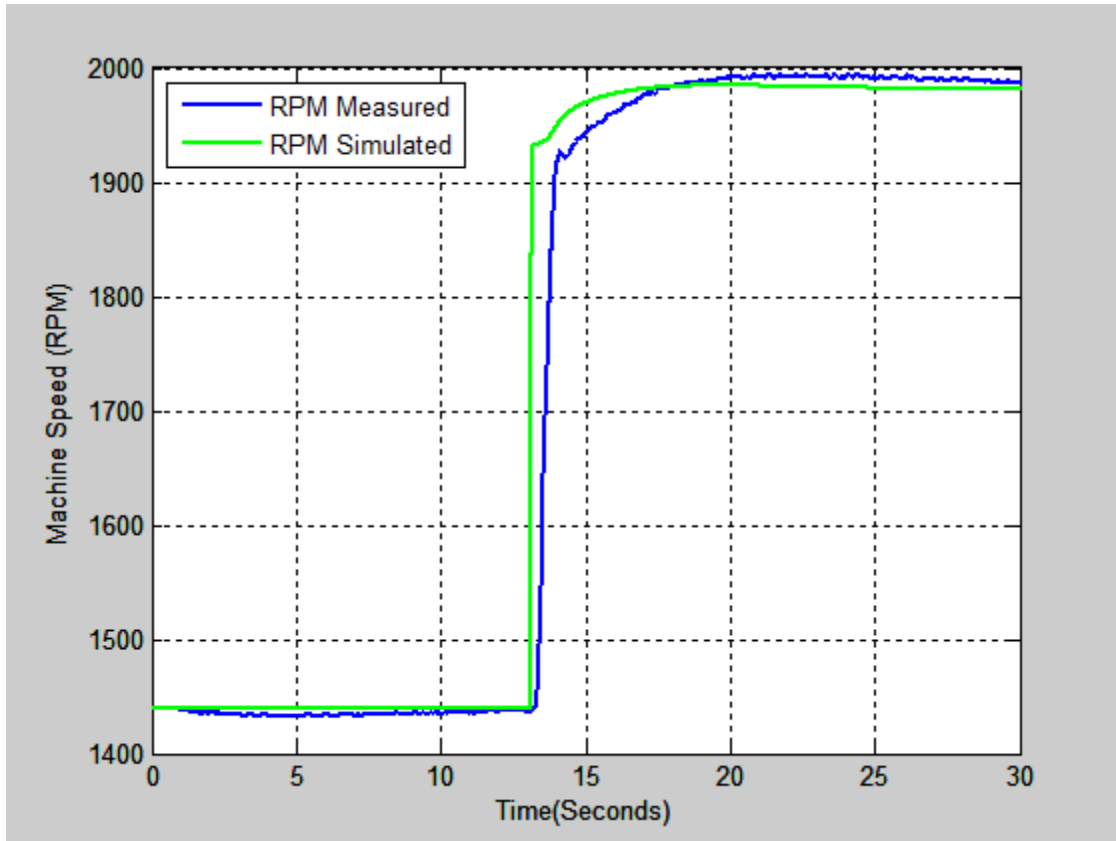


Figure 14.         Measured and simulated system RPM vs. time.

## 2.      Results

The data from the simulation compares very favorably with the operational speed. The simulated system responds more rapidly to the change in speed; however, there is little difference between the two operating sets at any point during the run.

The difference in response time is likely due to rapid response of the simulation versus the actual machine. The model constructed in Simulink is an ideal machine.

While inertia is accounted for in the data measured in earlier experiments, not all losses were accounted for. These particular components of the DC motor operation mute the response when compared to an ideal system.

## G.    MODEL VALIDATION FOR ELECTRICAL INPUT POWER

### 1.    Comparison between Operational Data and Simulated Data

The next step was validation of the simulation for the electrical input power to the armature of the DC motor. Input power was measured for the DC motor armature while operating the DFIG under the same conditions as the speed runs. The power, in watts, versus the time, in seconds, was plotted on the graph shown in Figure 15.



Figure 15.        Measured input power of DC motor vs. time.

17

The simulation was set to plot the output power data corresponding to the same set of conditions. Figure 16 is a display of the power input to the rotor versus time for the Simulink model. Both plots were placed on the same axes, found in Figure 17, for comparative analysis.



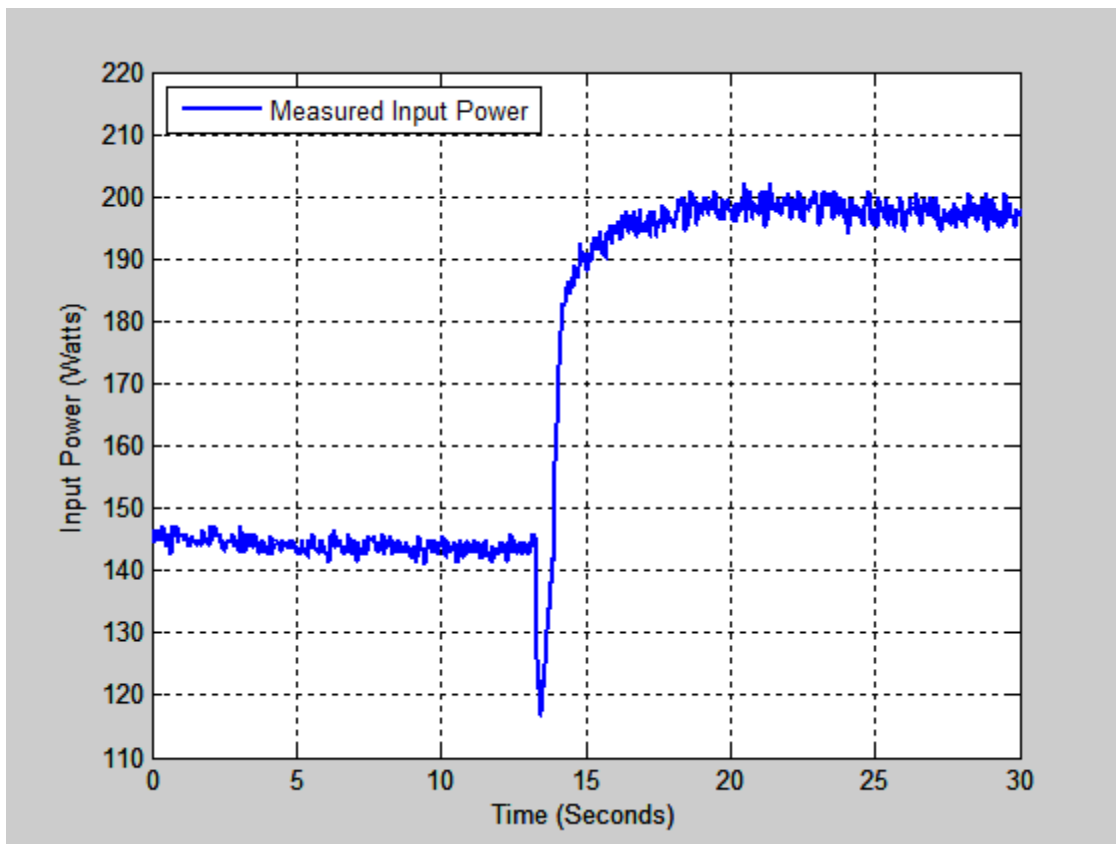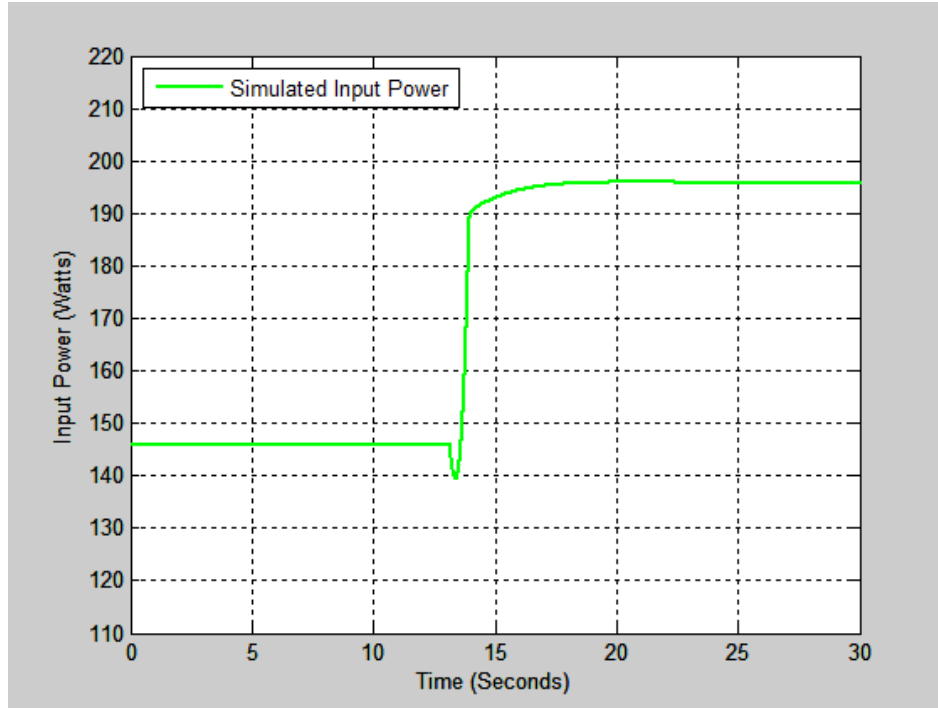Figure 16.    Simulated input power of DC motor vs. time.
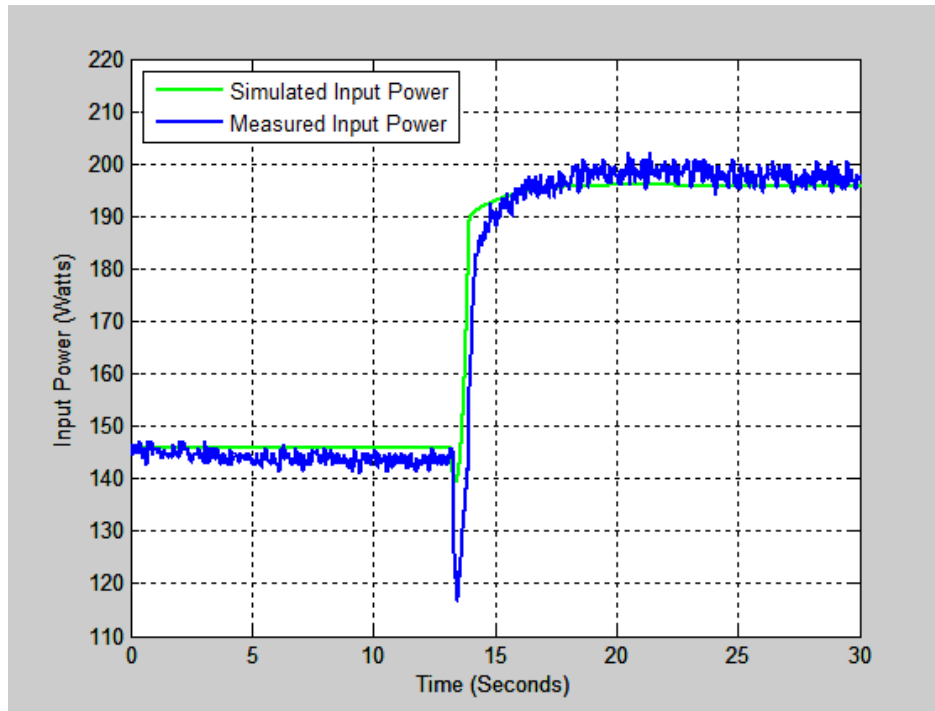
Figure 17.        Measured and simulated input power vs. time.

## 2.        Results

The simulated armature input power tracks well with the actual power profile supplied to the armature of the DC motor. However, the simulation assumes ideal characteristics. The change in speed causes a significant drop in input power (about 20%) before the power rises to a new, higher level. This drop-off, while present in the simulation, is not as pronounced. This is most likely caused by the simulation being able to respond instantaneously to changes in operational parameters, whereas the actual system cannot. The effect was produced in the simulation by adding a rate limiter at the output of the armature voltage to mute the response. The rate limiter prevented the drop in armature current from causing the voltage to surge to a higher value instantaneously.

During analysis, the armature self-inductance value in the simulation was lowered to 30 H. The result was a more rapid response to the change in speed. This alteration provided for a model that more accurately mimicked the machine behavior.

## H.    MODELING MECHANICAL OUTPUT POWER

After modeling the input power, attention was turned to creating an accurate simulation of the mechanical output power. Finding the output power required a theoretical approach due to the unavailability of the required equipment to measure the torque at the rotor. Therefore, certain assumptions were made to estimate the value of the output.

Windage and friction losses are present in any spinning machine [5]. However, there was no way to directly measure these values. The losses for the DC machine were considered to be limited to armature losses for this study. While not completely accurate, the simulated output is a much more realistic value for machine output power than assuming 100% efficiency between rotor input power and mechanical output power. The plot of the modeled output power, in watts, versus time, in seconds, for the speed transition between 1,441 and 1,981 RPM is found in Figure 18.
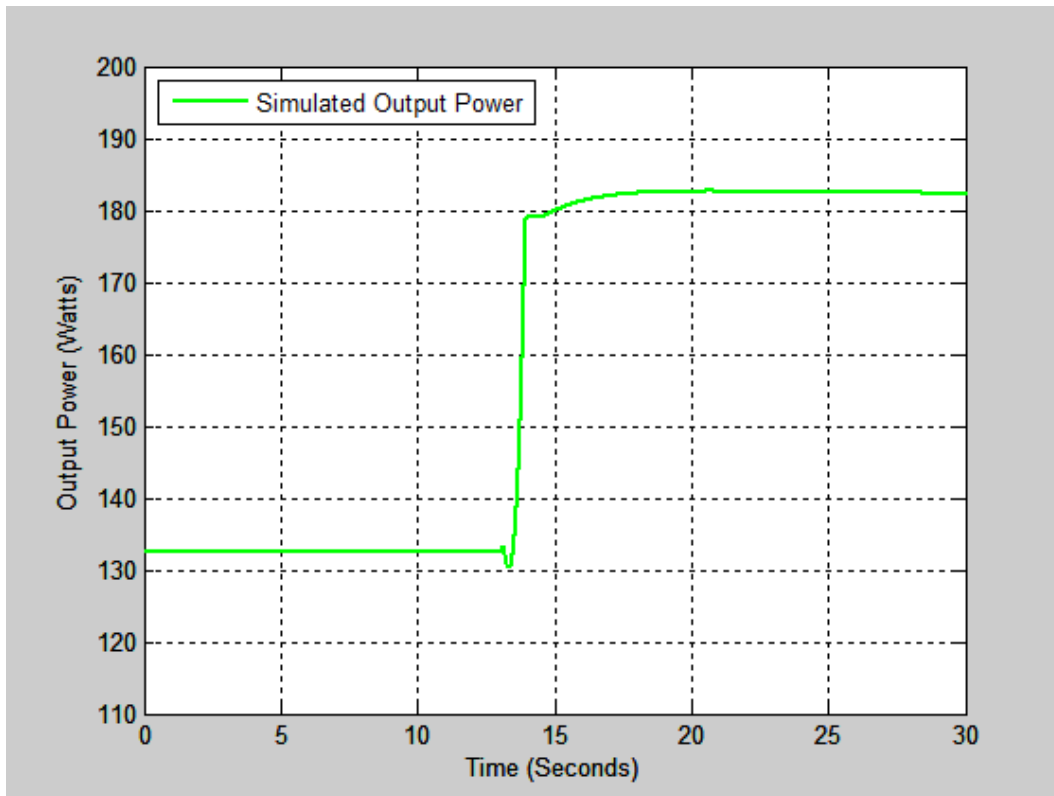


Figure 18.        Simulated output power of DC motor.

20

The output power is noticeably lower than the armature input power in Figure 17 when analyzing the same time period. Consideration of the armature losses causes this reduction.

## I.        CHAPTER SUMMARY

In this chapter, the DC motor operational theory was reviewed. The theory of operation was used as a basis to model a DC motor that was used as a torque input to a DFIG system simulation. Data was gathered from the operational system and compared to the simulation to determine whether system operation speed could be accurately predicted. Experimentation showed that the emulated speed was consistent with actual system operation.

The input power was also discussed. The resulting comparison found the simulation to accurately model of the rotational output power during steady state conditions. Transitions in speed caused disturbances in the input power that were not fully accounted for by the model. Overall, the model matches the operation of the machinery well. The next section uses this model to determine output power of the DC motor based on operating speeds derived from wind patterns within a particular region.

THIS PAGE INTENTIONALLY LEFT BLANK

# III. MODELING WIND PROFILES

## A. INTRODUCTION

Speed prediction has been shown to be accurate in our wind power emulator. The motor emulator can now be used to model the wind profiles of different geographic locations. The DC motor replaces the turbine and gearbox that act as the prime mover for a commercial wind turbine. By mapping the wind speeds in an area to the particular RPM of the DC machine, a particular wind profile of a region can be generated.

## B. MAPPING STRATEGY FOR WIND SPEED TO DC MOTOR SPEED

### 1. Overview

The process of determining the mapping procedure for wind speed to DC motor shaft RPM is covered in this section. The methodologies of assigning the numerical values of speed to the machine as well as the selection of the geographic area are discussed.

### 2. Geographic Area Selection

The geographic area was selected based on two factors. The first requirement was that the area be of significance to the DoD. This was done to tailor the research toward the goals of [1].

The second factor taken into consideration was the availability of wind speed data for the area. There are several military installations located throughout the nation. Not all of them have a significant amount of historical wind speed data readily available.

Viewing the problem from these two perspectives led to choosing Norfolk, Virginia as the area of study. There is a large amount of data archived by the National Climatic Data Center [6]. The data focused on for this study was the average wind speed. The information was held by the National Climatic Data Center was compiled over a 54-year period. The monthly and annual average wind speeds are present.

The monthly data from [6] is presented in Table 2. Average wind speed is given in miles per hour (MPH).

Table 2.    Monthly wind speed averages for Norfolk, Virginia, from [6].

| Norfolk, Virginia | |
| --- | --- |
| **Month** | **Average Wind Speed (MPH)** |
| January | 11.4 |
| February | 11.8 |
| March | 12.3 |
| April | 11.8 |
| May | 10.4 |
| June | 9.7 |
| July | 8.9 |
| August | 8.8 |
| September | 9.6 |
| October | 10.2 |
| November | 10.3 |
| December | 10.9 |

The maximum average wind speed, by month, occurs in March at 12.3 MPH. The minimum average wind speed is 8.8 MPH in August. It was necessary to develop a mapping scheme that was able to encompass all of these speeds.

**3.    Mapping Strategy**

The machine speed for commercial wind turbines is varied according to the wind speed. As a result, maximum power conversion is performed at all speeds. The ideal

machine speed for a particular turbine and gearbox combination follows a peak power curve as a function of wind speed and turbine speed [2]. To simplify the model, the curved was linearized.

It was decided to set the maximum motor speed equal to a wind speed of 13 MPH. The motor speed was then scaled for the average monthly wind speed proportionally using

$$RPM_o = S_M \times \frac{2000 \text{ RPM}}{13 \text{ MPH}}$$ (2.10)

where $RPM_O$ is the operating speed for the system in RPM and $S_M$ is the average monthly wind speed in MPH. The results of the scaling are found in Table 3.

Table 3.    Scaling of monthly average wind speed in Norfolk, Virginia, to motor RPM.

| **Month** | $S_M$ | $RPM_O$ |
|-----------|-------|---------|
| January | 11.4 | 1754 |
| February | 11.8 | 1815 |
| March | 12.3 | 1892 |
| April | 11.8 | 1815 |
| May | 10.4 | 1600 |
| June | 9.7 | 1492 |
| July | 8.9 | 1369 |
| August | 8.8 | 1354 |
| September | 9.6 | 1477 |
| October | 10.2 | 1569 |
| November | 10.3 | 1585 |
| December | 10.9 | 1677 |

The value of $RPM_O$ was rounded to the nearest whole number to facilitate easier calculations. Information from this data set was used as part of the validation of the simulation as a model for wind speed.

## 4. Simulation of Different Wind Speeds

The motor speeds derived from the mapping were input into the simulation to replicate the different average wind speeds across each month in Norfolk. The associated output power levels for the machine speeds were plotted. In Figure 19, $RPM_O$ is plotted versus time for each month. The simulation speed begins at 1,754 RPM to represent the month of January. Every four seconds, $RPM_O$ is shifted to that of each subsequent month.
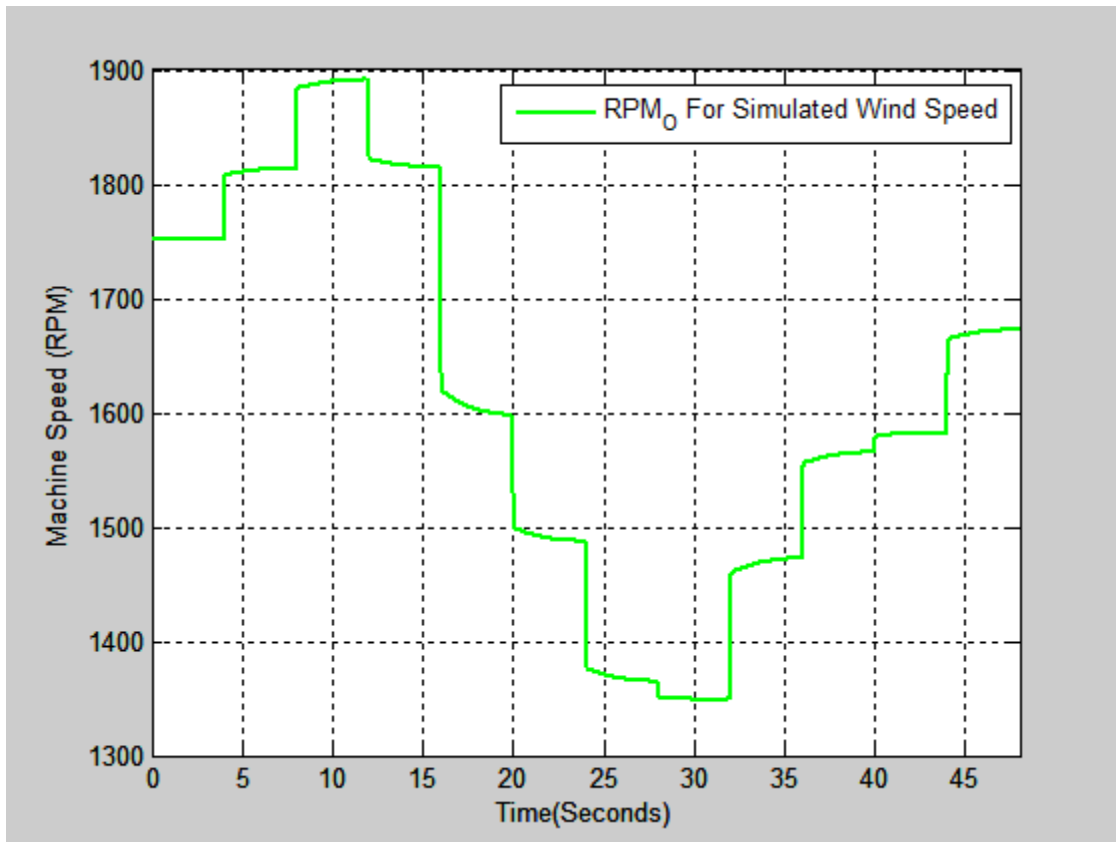


Figure 19.     Simulated average DC motor speed by month for wind turbine in Norfolk.

## 5. Simulation of Output Power Based on Wind Speeds

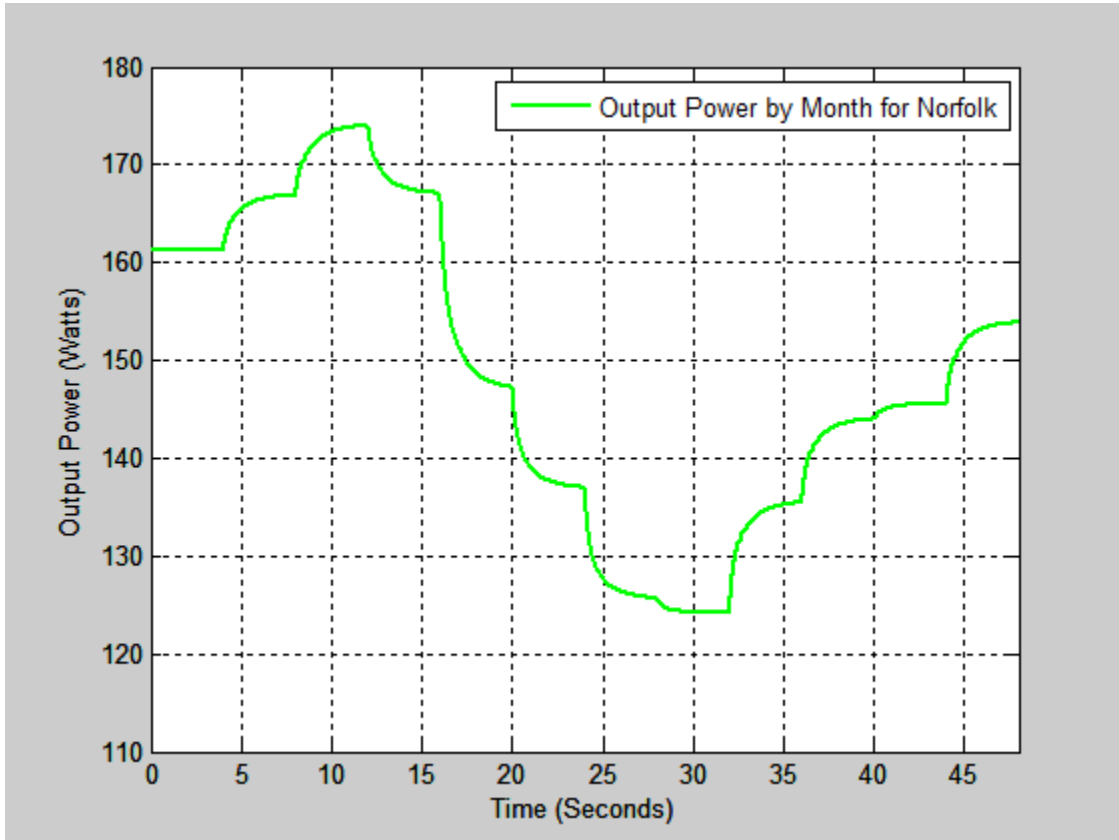The output power produced by the simulation was graphed in Figure 20.

Figure 20.        Simulated average DC motor output power by month for Norfolk.

The changes in power are organized in the same manner as the changes in speed. The power begins with the value corresponding to the month of January. The value of $RPM_O$ is adjusted every four seconds according the month represented. This led to the variations in power level seen in the plot. The steady state power at each change in speed indicates the predicted output power of the machine for that speed.

6.        **Analysis of Simulated Speed and Power**

The plots contained within this chapter illustrate the scenarios of speed and power production. The correlation between the speed of operation and the mechanical output power was proven through the data plots. Simulated monthly power was almost directly proportional to the speed.

The plot of power does not instantly jump to the final value based on the speed. This is due to the rate limiter installed in the circuit for the voltage. The behavioral traits of the machine are shown on the graph and, therefore, it takes a finite amount of time to reach a new output power. The transition time of four seconds allows the model to reach a steady state value of power for the given speed before transitioning to the next value.

## C.    CHAPTER SUMMARY

In this chapter, a mapping strategy was devised for converting wind speed to rotational speed of the DC motor. The simulation was run using the mapped speeds as a basis for commanded speed changes. Output power of the machine was calculated based on the simulated operating speeds.

The correlation between the rotational speed and mechanical output power of the DC machine was proven. This model can now be adjusted for specific scenarios in operational speed. Conclusions to the study and further research options are discussed in the next chapter.

# IV. CONCLUSIONS AND FUTURE RESEARCH

## A. CONCLUSIONS

In this thesis, the theory behind the operation of DC motors was reviewed. Understanding of this theory allowed for the creation of a Simulink model representing a separately excited DC motor. Testing was completed to validate the model outputs of speed and rotational power. Using wind speeds mapped to the RPM of the machine, we showed how the output power of the DC motor varied with the speed of the machine.

## B. FUTURE RESEARCH

The DC motor used can be modeled in greater detail. Slew rate limiting of the applied armature voltage was added and improved the prediction of the simulation compared to the measured results. The physics behind this behavioral model should be explored further. This would allow for a more accurate profile of the machine that models the responses more faithfully.

A separate study should also measure the output of the DFIG to compare against the output of the DC motor. The relationship between the two should be detailed. The theoretical output of a larger system, such as those used in wind turbines, can be scaled from the data obtained.

Future work should also include matching the DC machine to specific wind turbine blades and gearboxes. The output power in this thesis uses a linearized model to convert wind speed to machine speed. For an actual wind turbine, the ideal operating points are based on a curve [2]. By modeling the curve, behavior of a specific combination of turbine blades and gearbox can be analyzed.

THIS PAGE INTENTIONALLY LEFT BLANK

# APPENDIX A

## Lab-Volt DC Machine
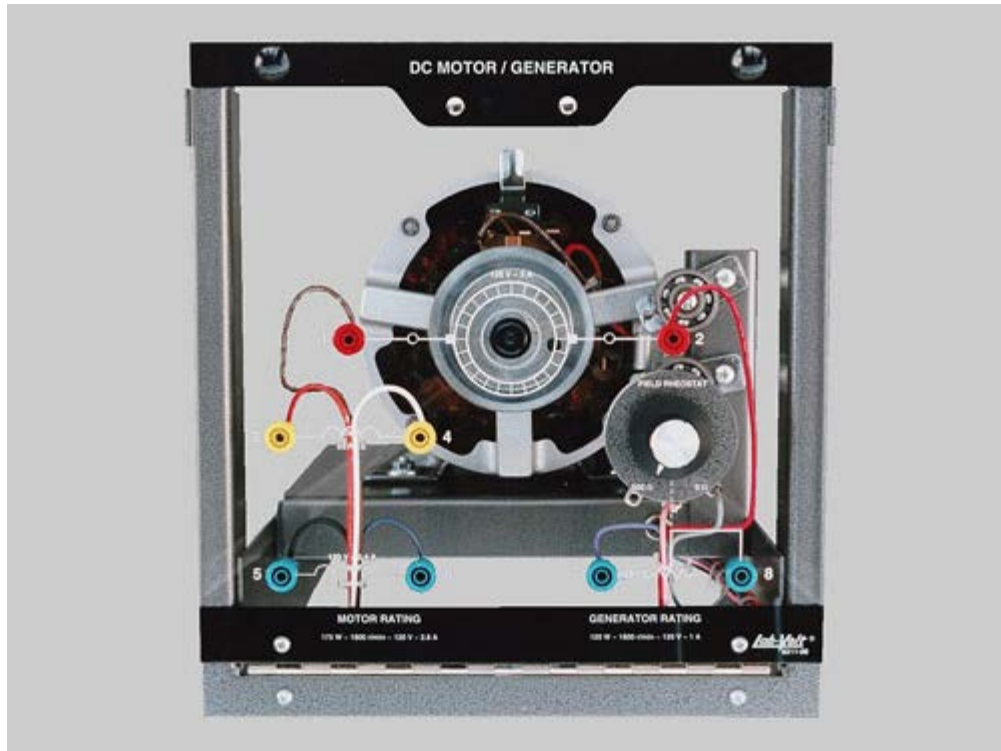


This machine can be run independently as a DC motor or a DC generator. The armature, shunt field, and series field windings are terminated separately on the faceplate to permit long and short shunt as well as cumulatively and differentially compounded motor and generator connections. This machine is fitted with exposed movable brushes to allow students to study the effect of armature reaction and commutation while the machine is operating under load. An independent, circuit-breaker protected, shunt-field rheostat is mounted on the faceplate for motor speed control or generator output voltage adjustment.

| Model 8211 – DC Motor/Generator | | 120/208 V – 60 Hz | 220/380 V – 50 Hz | 240/415 V – 50 Hz |
|---|---|---|---|---|
| Power Requirement | | 120/208 V | 220/380 V | 240/415 V |
| Rating | Motor Output Power | 175 W | | |
| | Generator Output Power | 120 W | 110 W | 120 W |
| | Armature Voltage | 120 V – DC | 220 V – DC | 240 V – DC |
| | Shunt Field Voltage | 120 V – DC | 220 V – DC | 240 V – DC |
| | Full Load Speed | 1800 r/min | 1500 r/min | 1500 r/min |
| | Full Load Motor Current | 2.8 A | 1.3 A | 1.1 A |
| | Full Load Generator Current | 1 A | 0.5 A | 0.5 A |
| Physical Characteristics | Dimensions (H x W x D) | 308 x 291 x 440 mm (12.1 x 11.5 x 17.3 in) | | |
| | Net Weight | 14.1 kg (31 lb) | | |

# APPENDIX B

## Simulink Model Files

Induction Machine model A.Julian, 20 May 08
Operating as an Asynchronous Generator

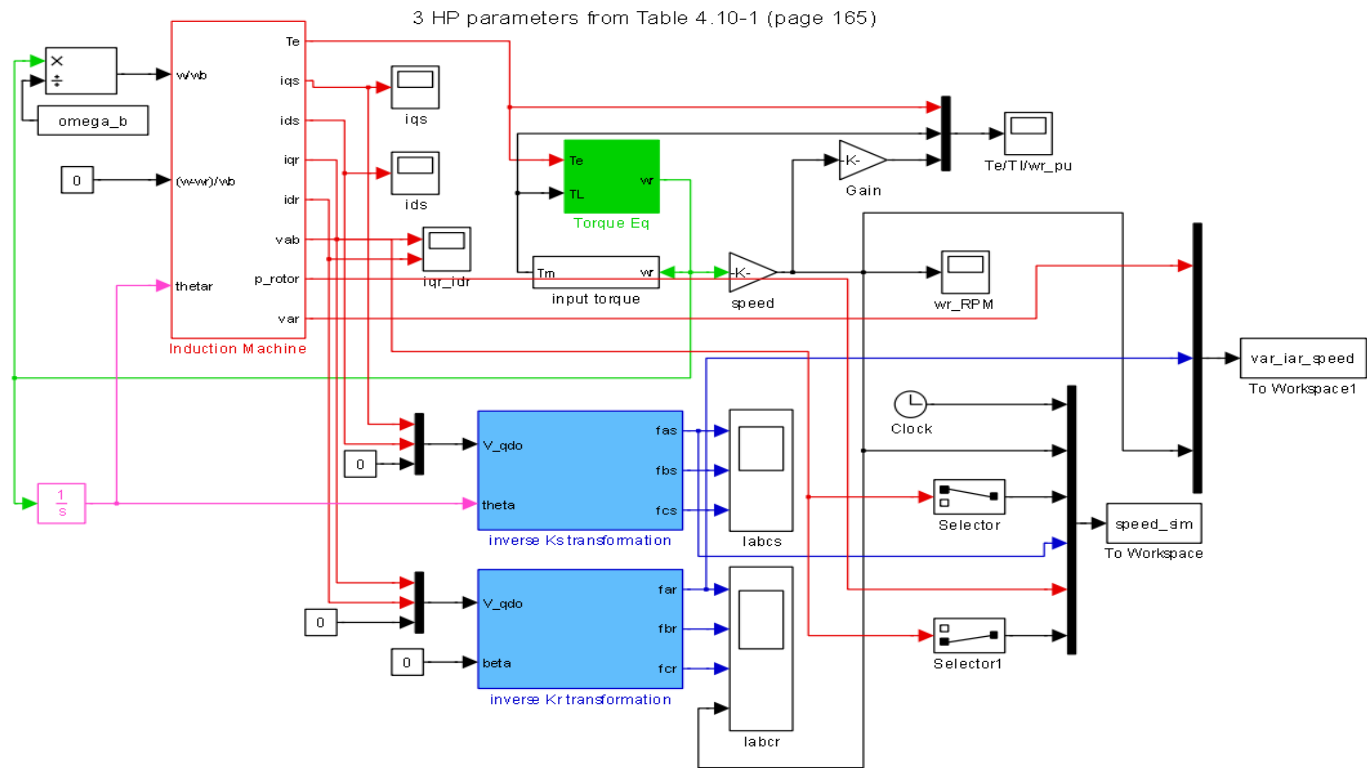Equations: 4.14-1 to 4.14-19 in Krause text
Torque Eq. 4.3-8

3 HP parameters from Table 4.10-1 (page 165)



Figure 21.        Overall DFIG system, from [3].
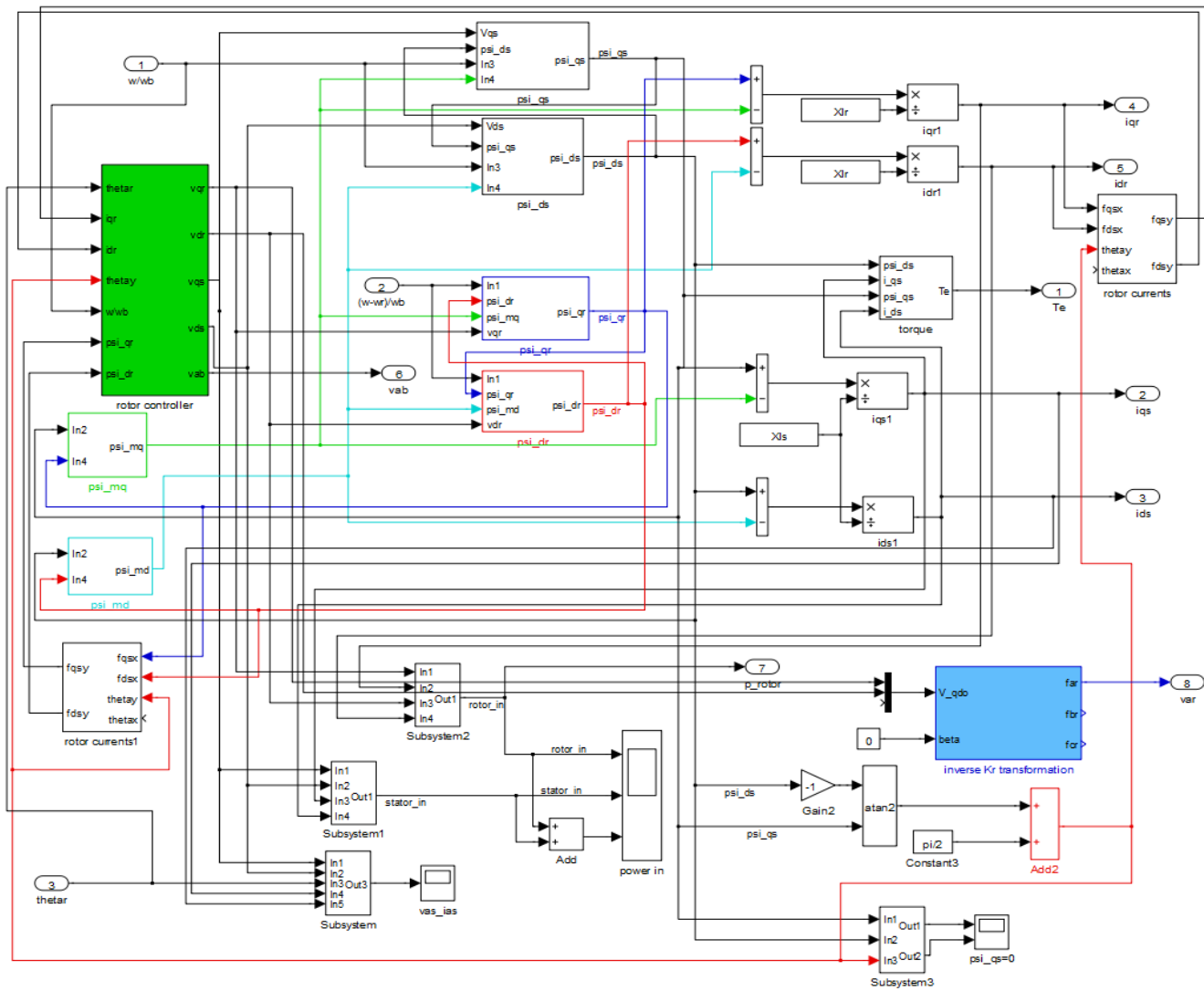
33

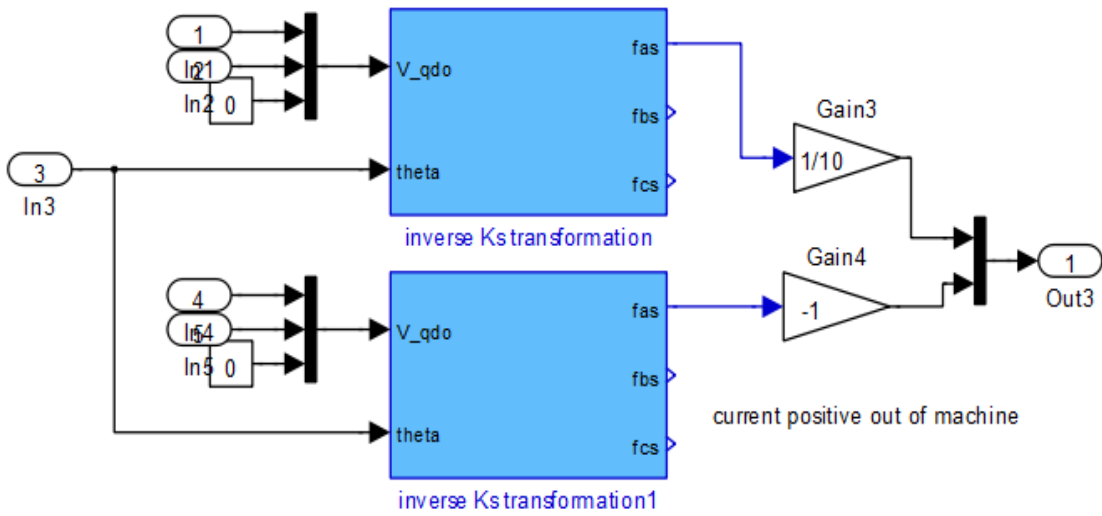Figure 22.        Induction Machine of Overall DFIG system, from [3].

Figure 23.        Subsystem of Induction Machine, from [3].
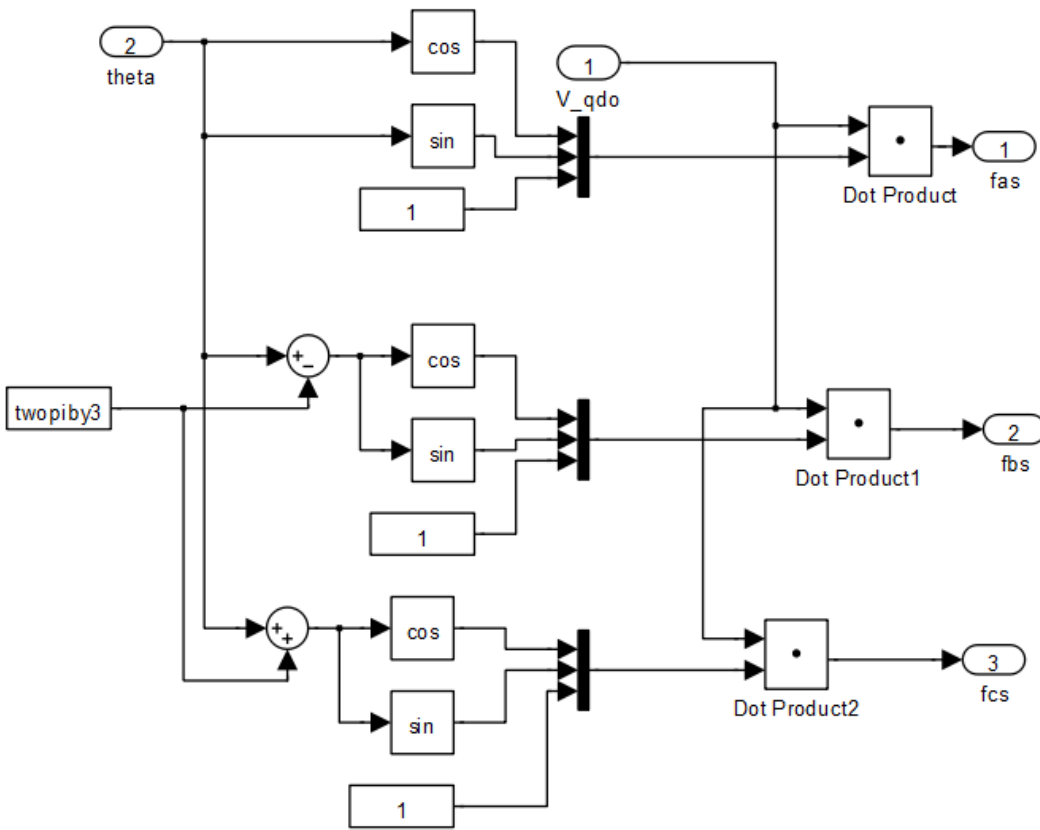


Figure 24.        Inverse Ks transformation in Subsystem, from [3].

35
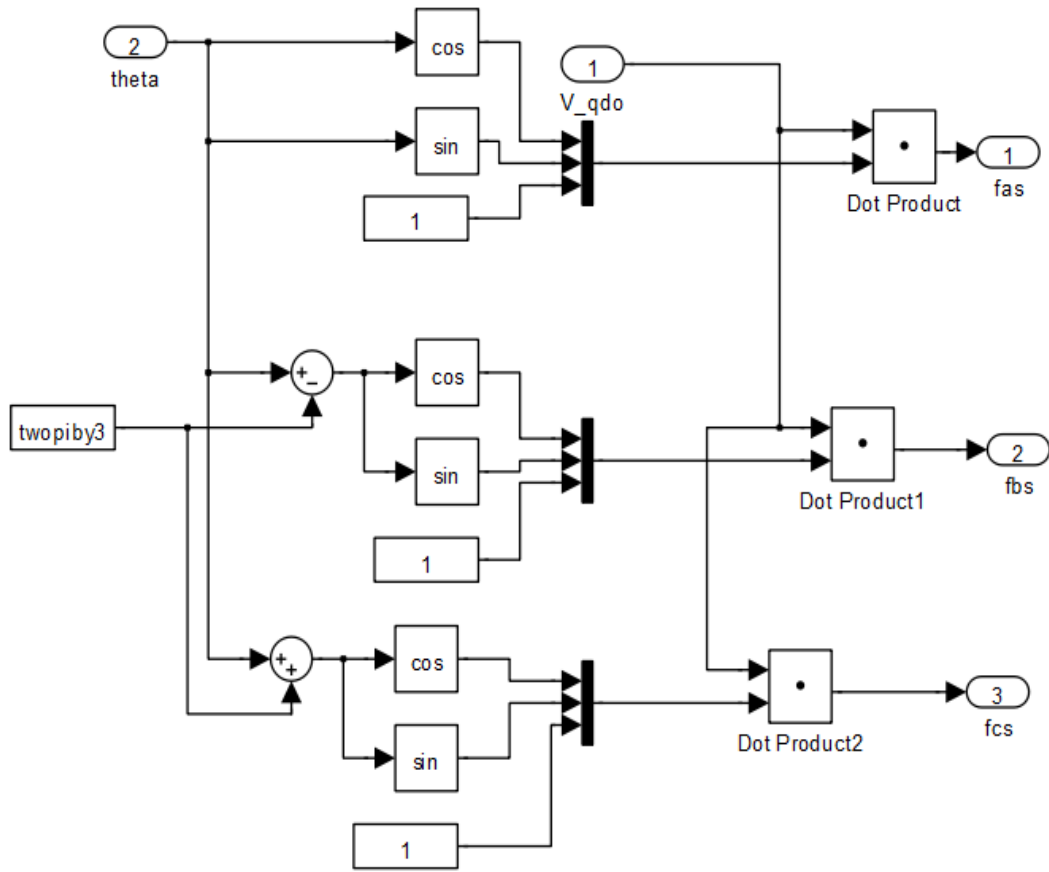
Figure 25.    Inverse Ks transformation1 in Subsystem, from [3].
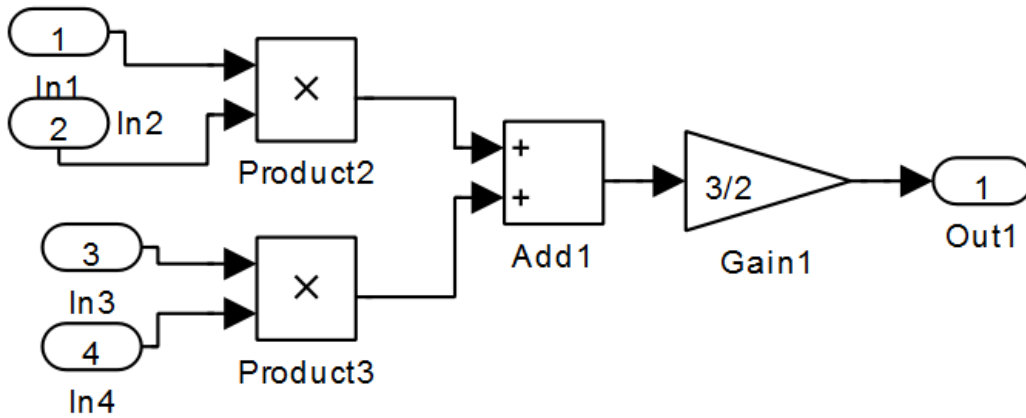
Figure 26.          Subsystem1 of Induction Machine, from [3].
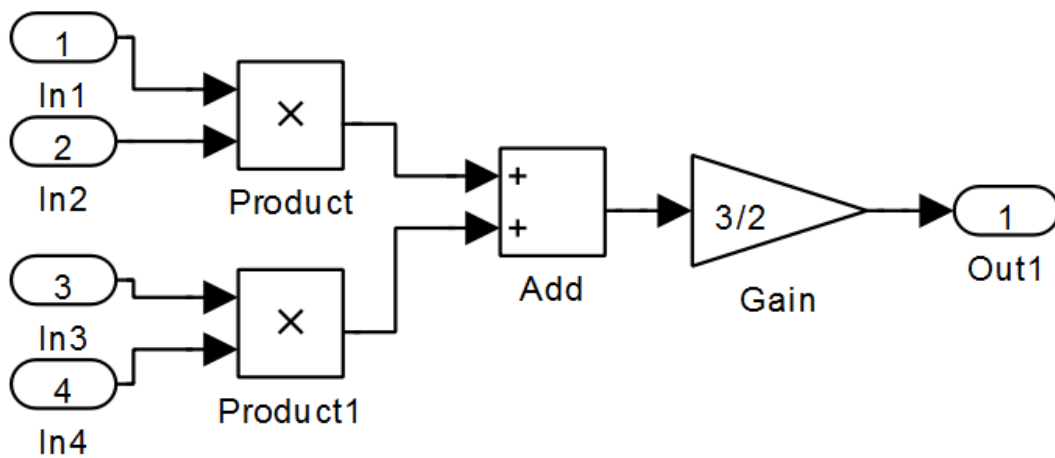


Figure 27.          Subsystem2 of Induction Machine, from [3].
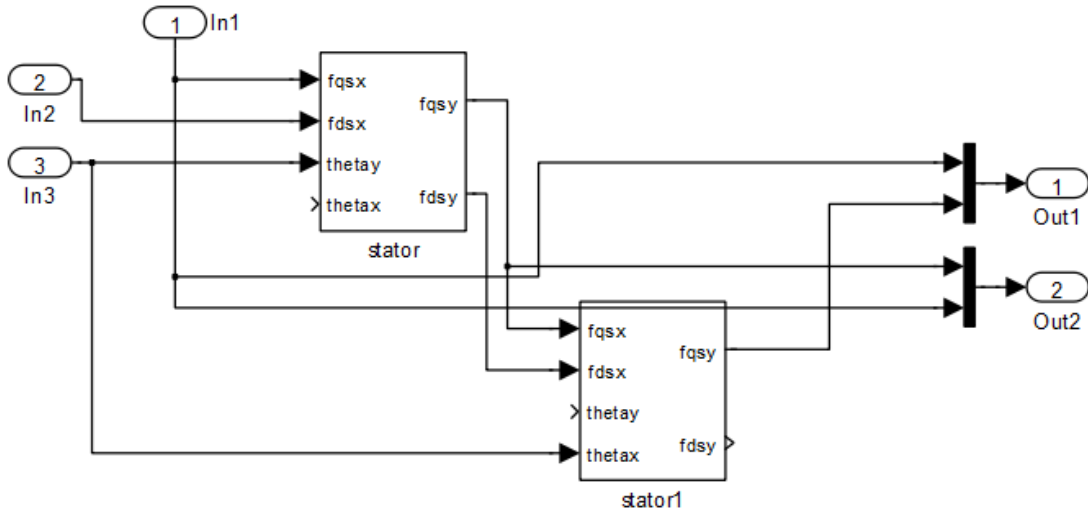
Figure 28.        Subsystem3 of Induction Machine, from [3].
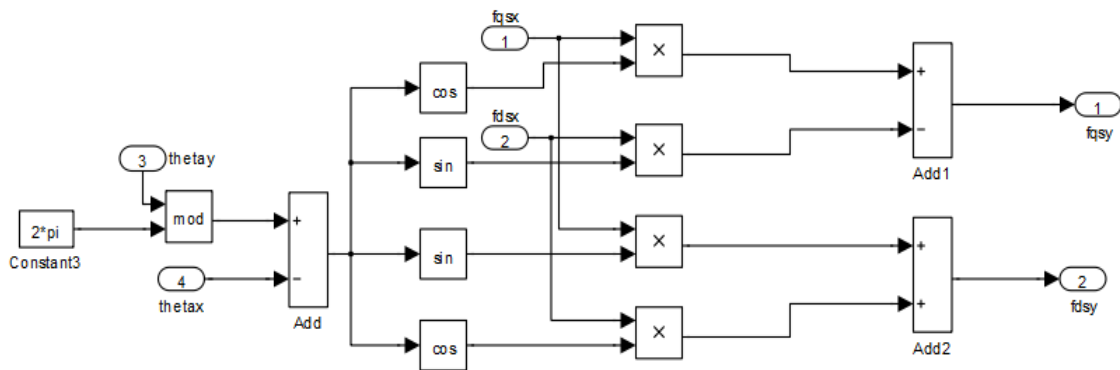


Figure 29.        Stator of Subsystem3, from [3].

38
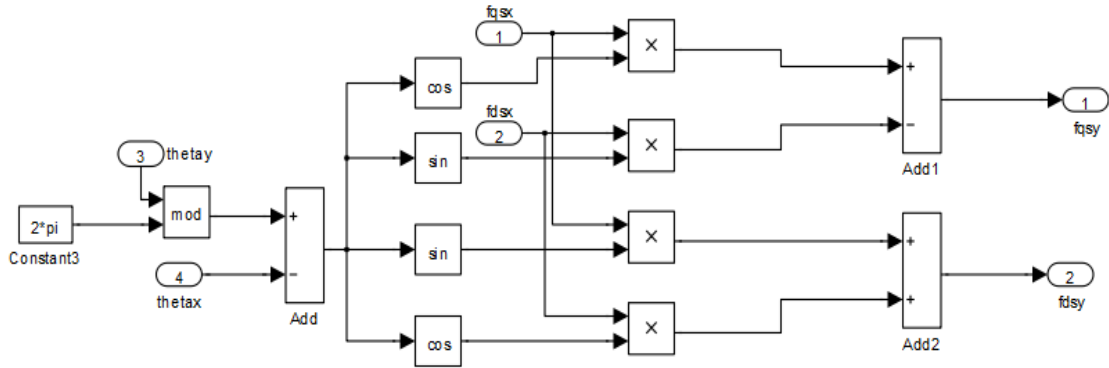
Figure 30.        Stator1 of Subsystem3, from [3].
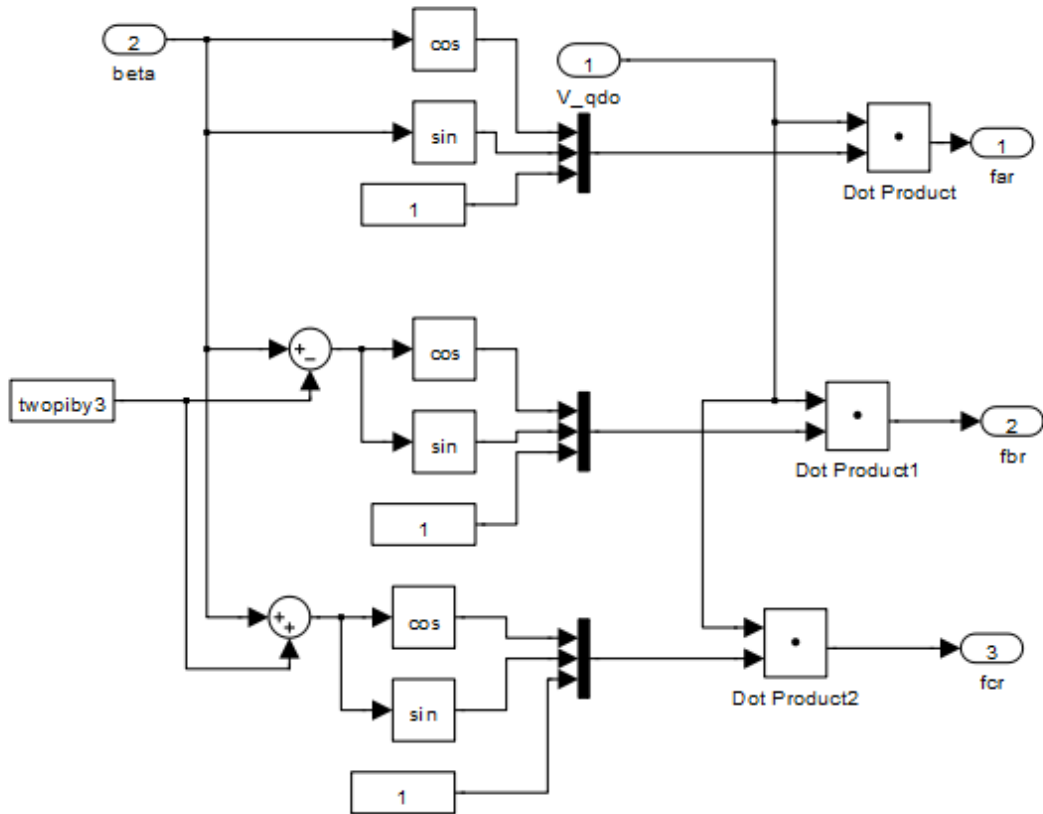


Figure 31.        Inverse Kr transformation of Induction Machine, from [3].
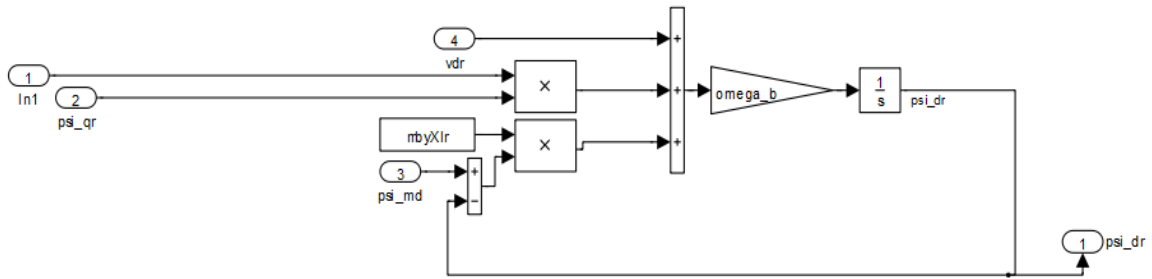
Figure 32.        Psi_dr of Induction Machine, from [3].
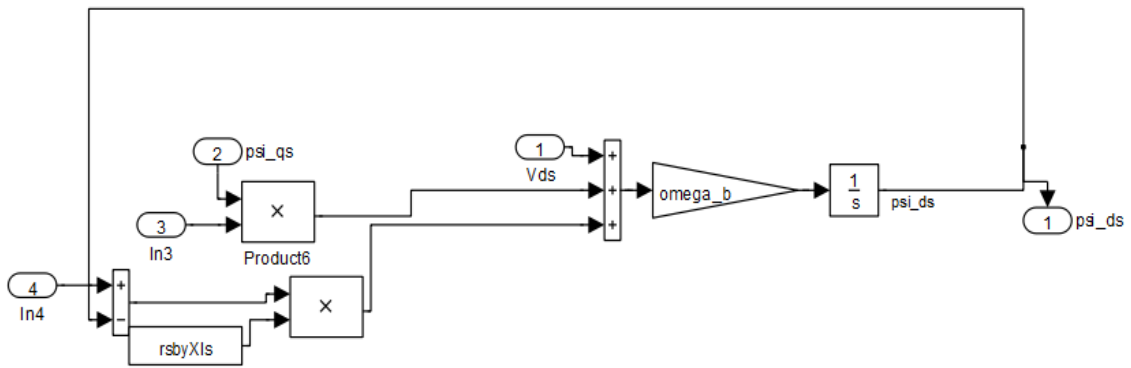


Figure 33.        Psi_ds of Induction Machine, from [3].
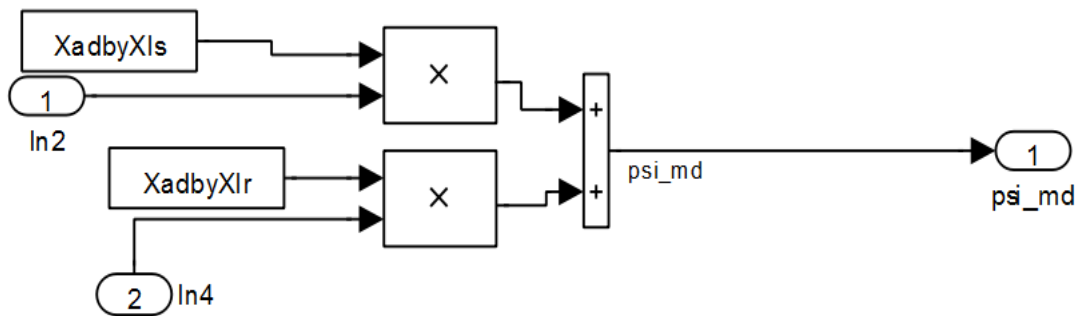


Figure 34.        Psi_md of Induction Machine, from [3].
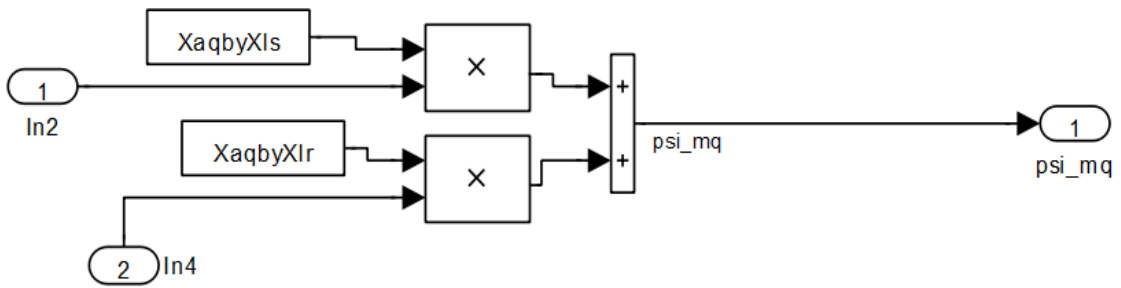
Figure 35.        Psi_mq of Induction Machine, from [3].
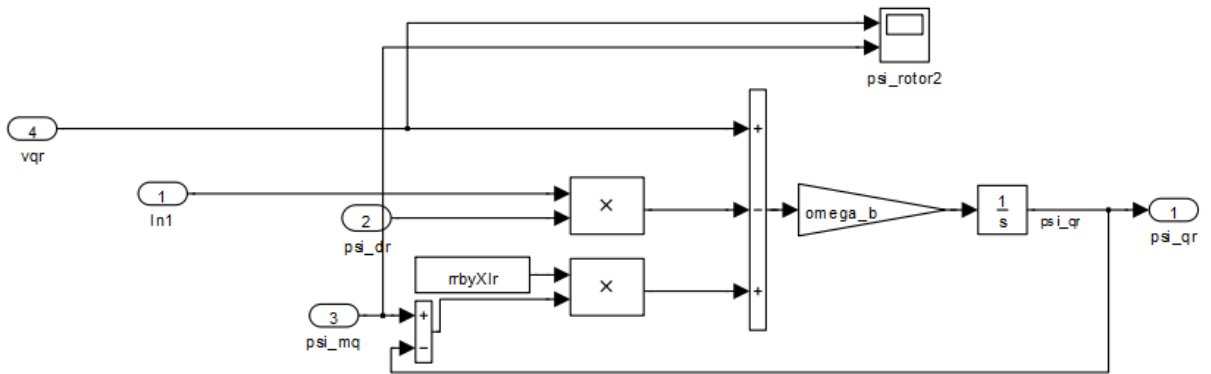


Figure 36.        Psi_qr of Induction Machine, from [3].
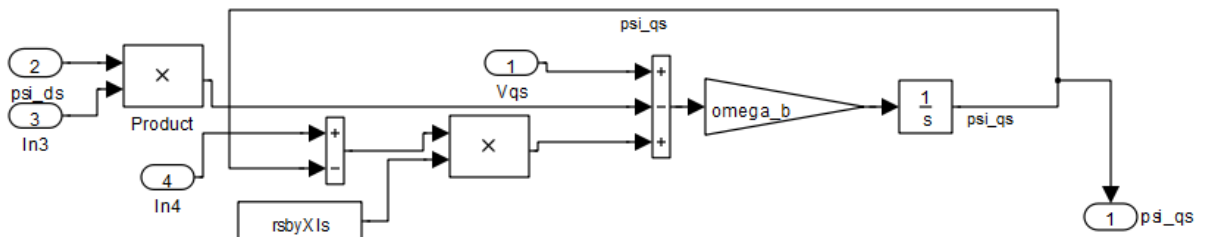


Figure 37.        Psi_qs of Induction Machine, from [3].
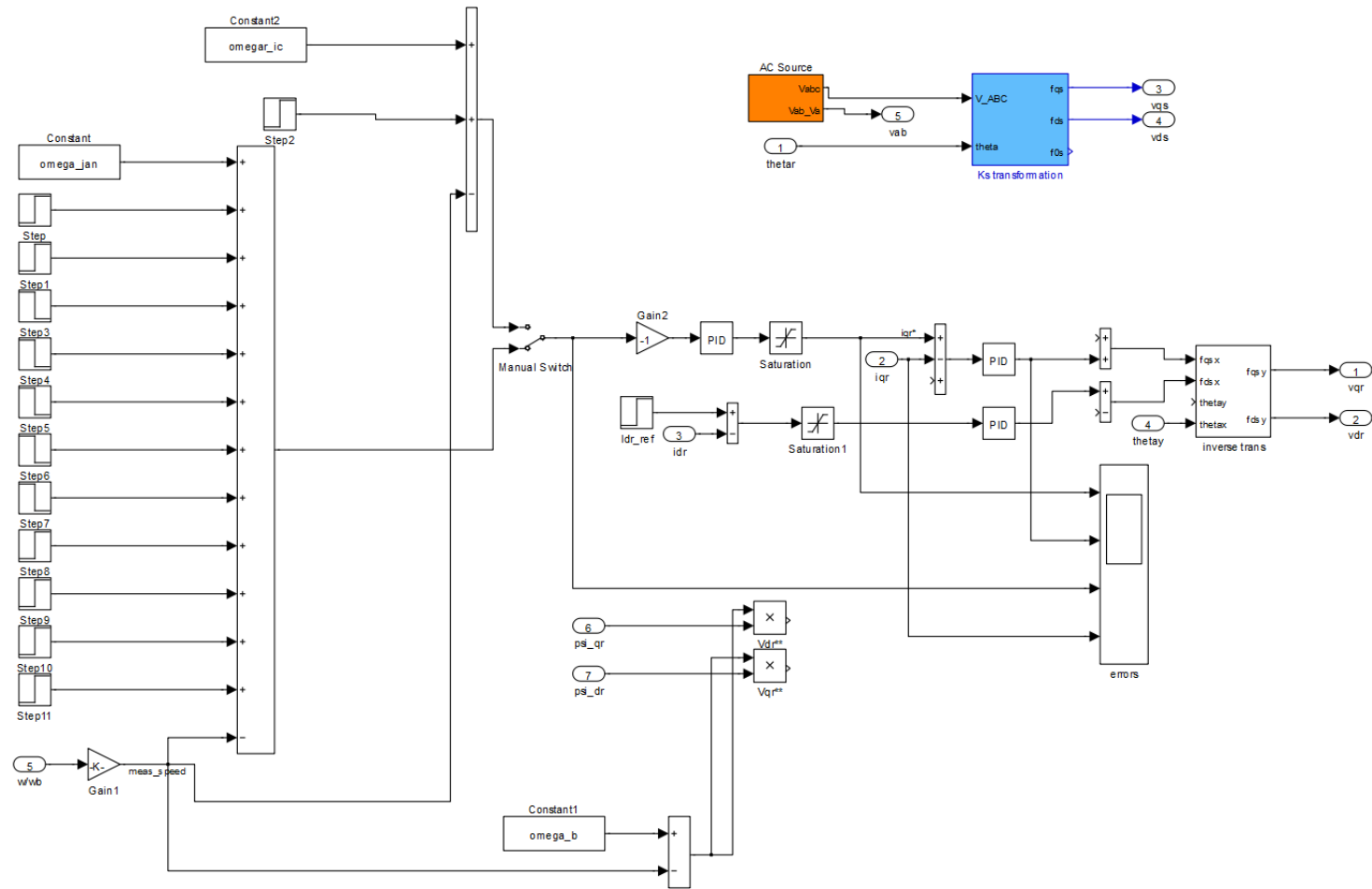
Figure 38.        Rotor controller of Induction Machine, from [3].
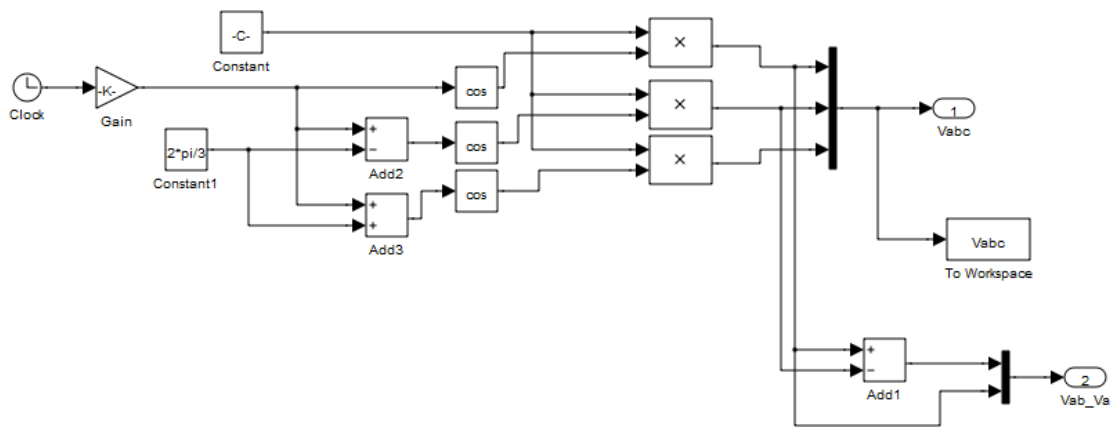
Figure 39.        AC source of Rotor Controller, from [3].
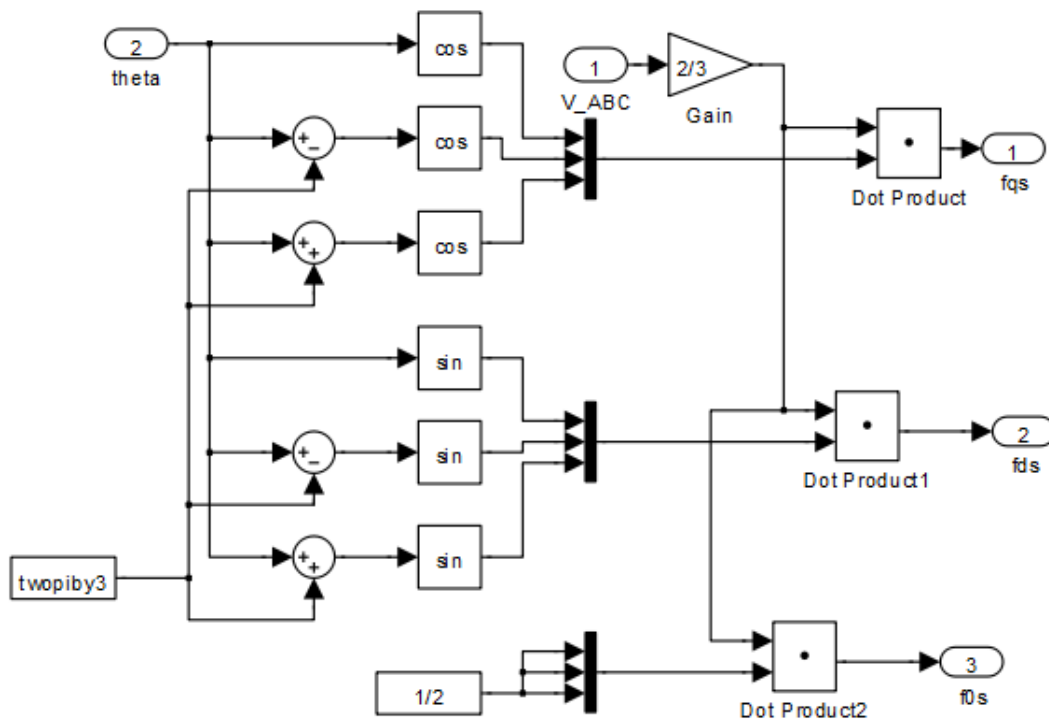


Figure 40.        Ks transformation of Rotor Controller, from [3].
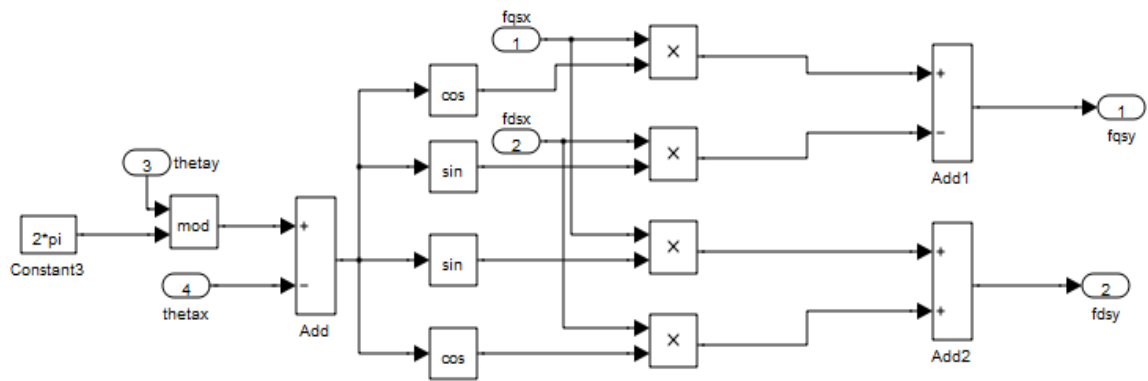
Figure 41.          Inverse trans of Rotor Controller, from [3].
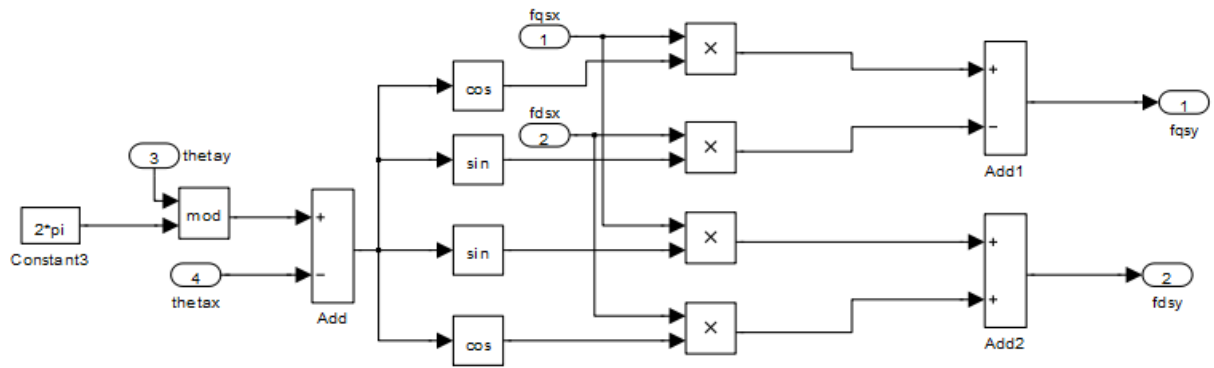


Figure 42.          Rotor currents of Induction Machine, from [3].
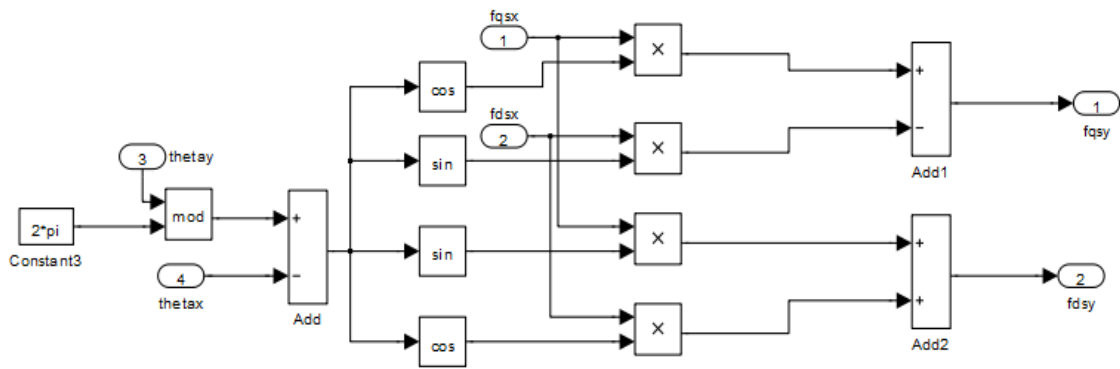
Figure 43.          Rotor currents1 of Induction Machine, from [3].
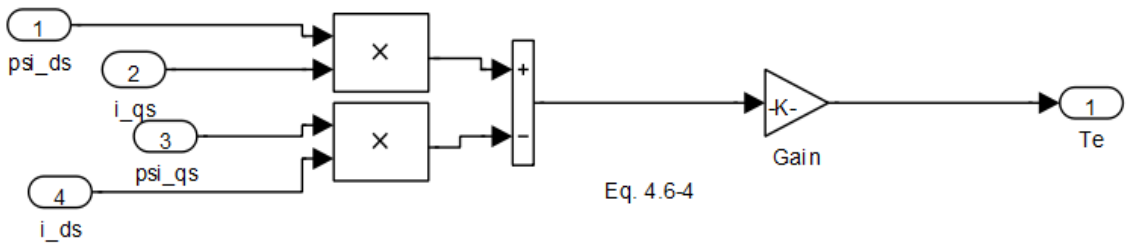


Figure 44.          Torque of Induction Machine, from [3].

45
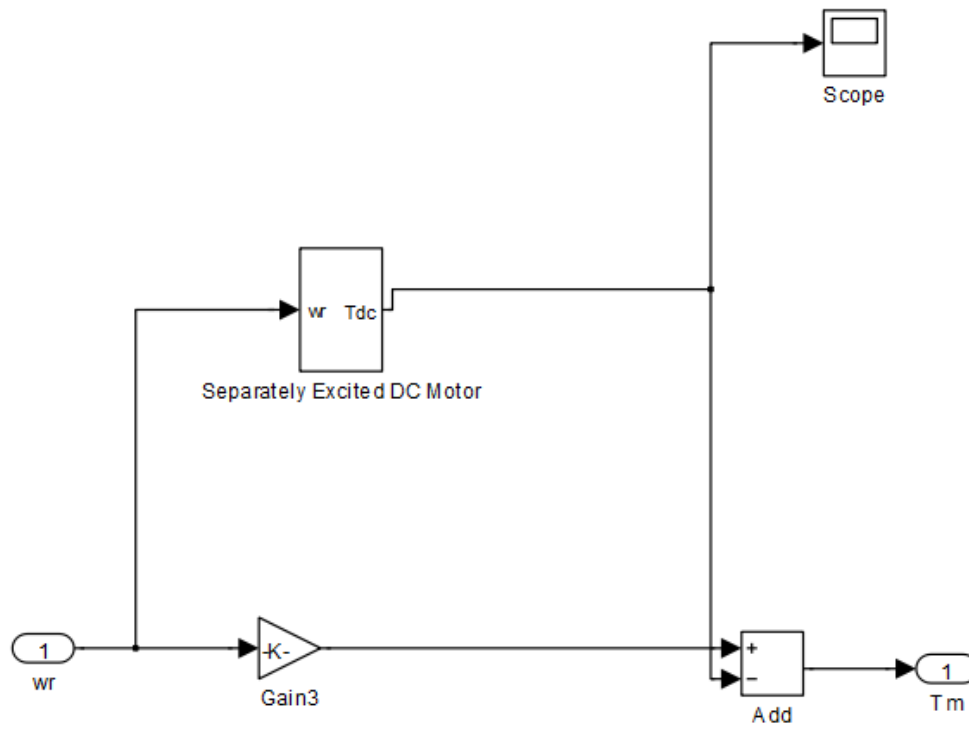
Figure 45.        Input torque of Overall DFIG system.
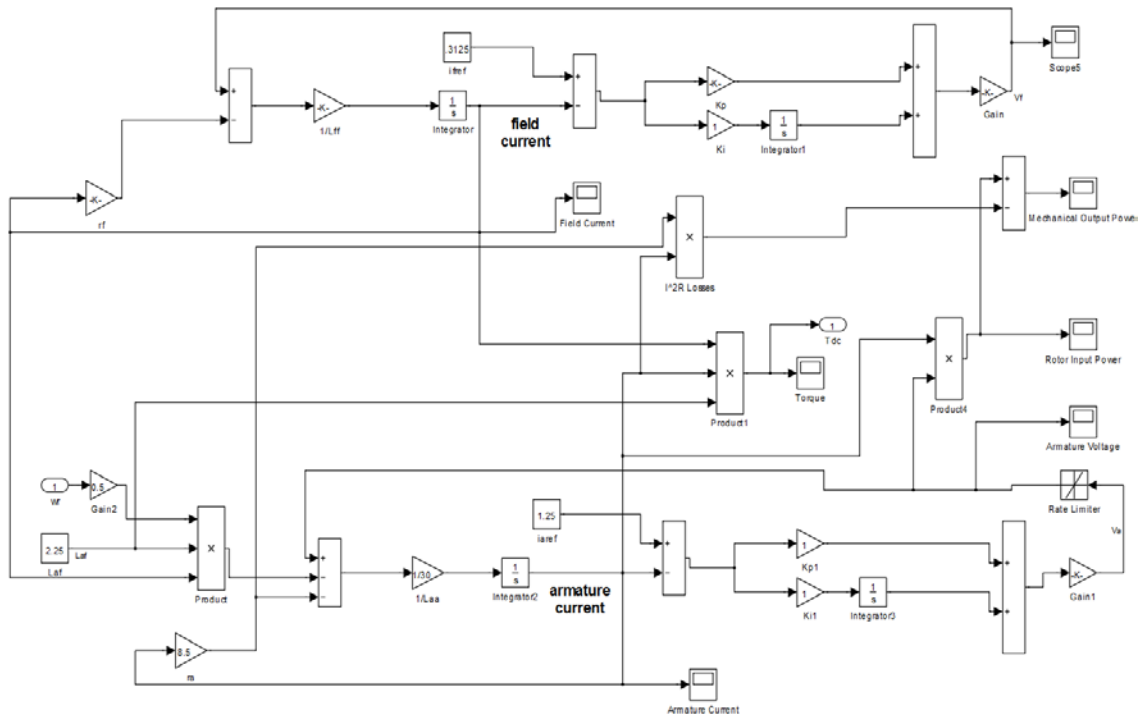
Figure 46.    Separately excited DC motor of input torque.
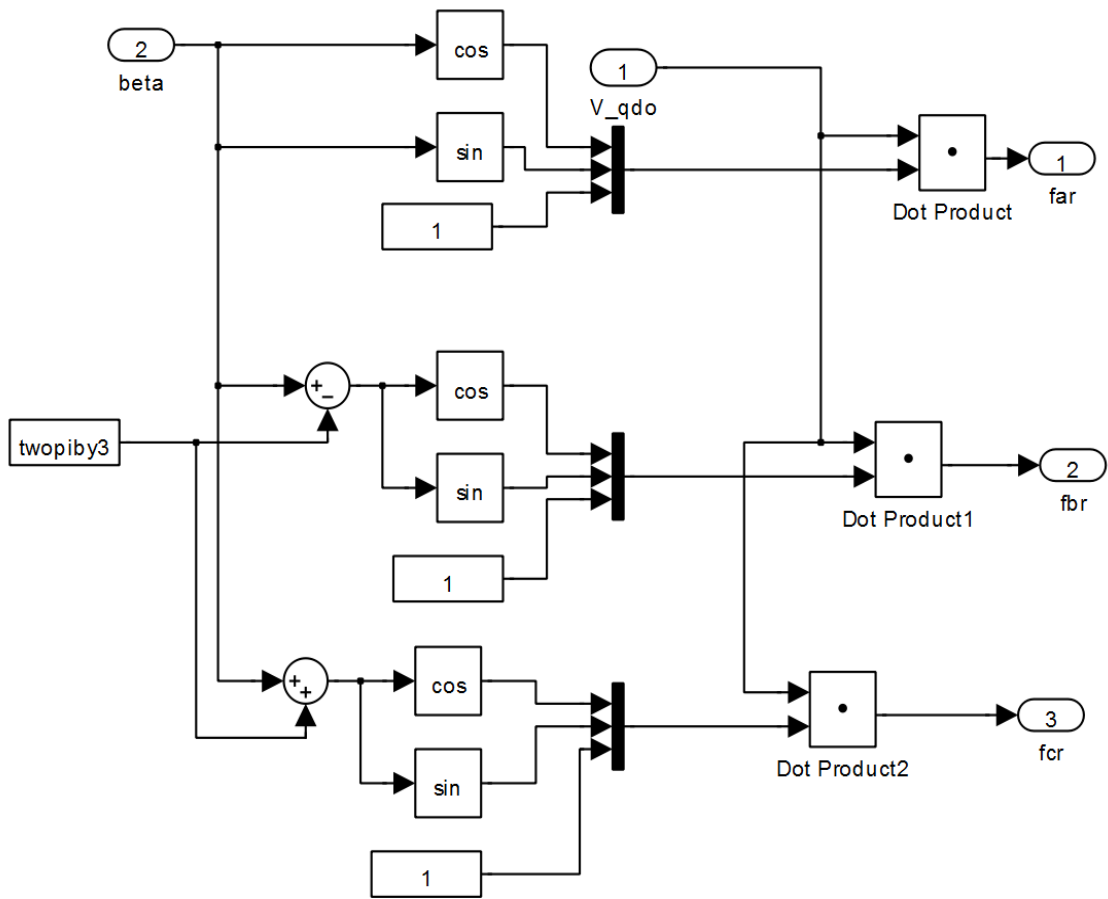
Figure 47.　　Inverse Kr transformation of Overall DFIG system, from [3].
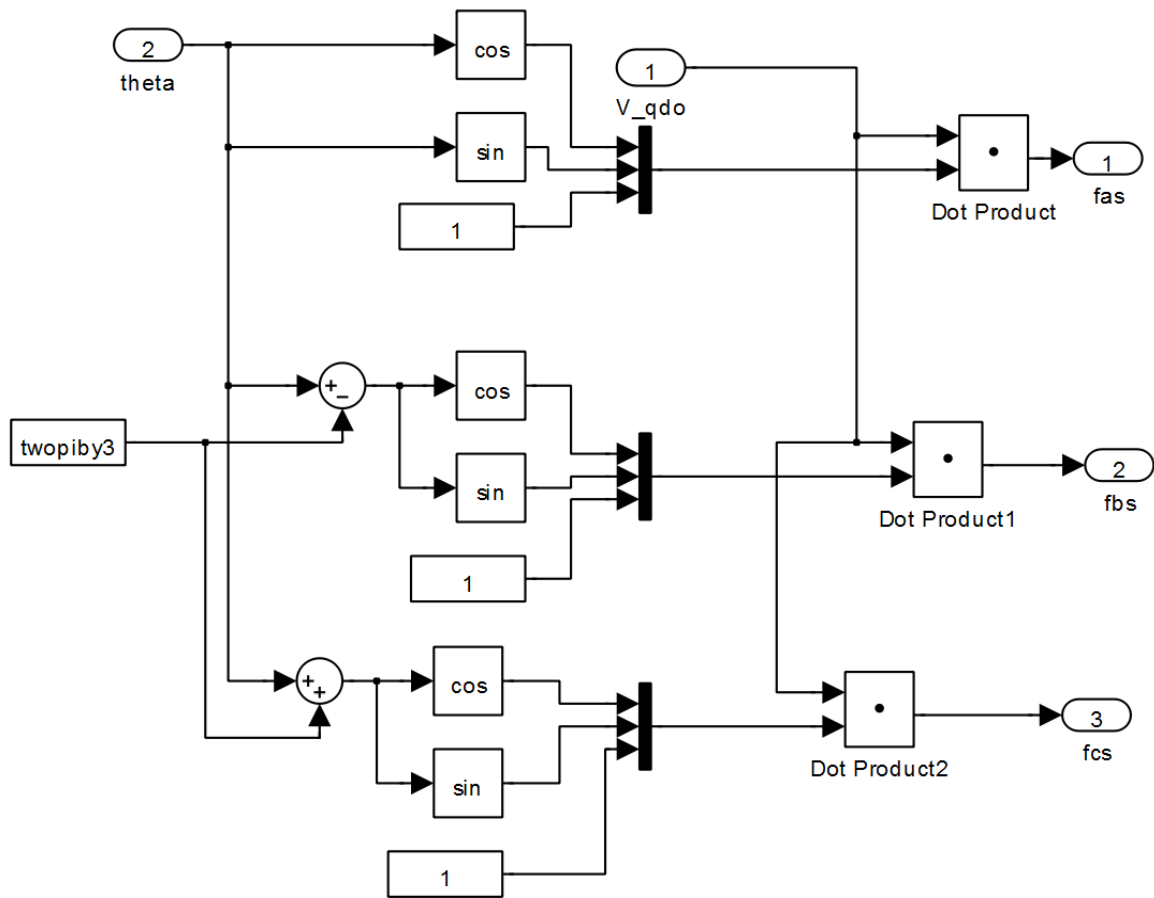
Figure 48.        Inverse Ks transformation of Overall DFIG system, from [3].
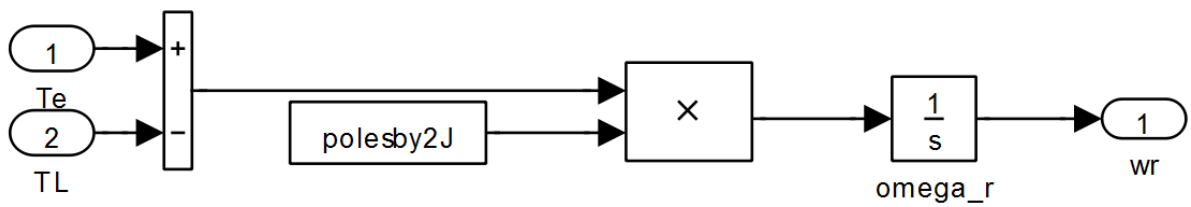


Figure 49.        Torque equation of Overall DFIG system, from [3].

THIS PAGE INTENTIONALLY LEFT BLANK

# APPENDIX C

## Matlab M-Files

**Plot_recorder_update.m**

```matlab
% Jonathan Hines Jan12
clear all;
omega_b = 2*pi*60;


%---------------------------------------------
omegar_ic = omega_b*0.8;     %1441 RPM; used for initial tests
omega2=omega_b*0.3;


omega_jan=367;                    %used for monthly power data; replace in
model
omega_feb=0.035*omega_jan;
omega_mar=0.044*omega_jan;
omega_apr=-0.044*omega_jan;
omega_may=-0.123*omega_jan;
omega_jun=-0.062*omega_jan;
omega_jul=-0.070*omega_jan;
omega_aug=-0.009*omega_jan;
omega_sep=0.070*omega_jan;
omega_oct=0.052*omega_jan;
omega_nov=0.009*omega_jan;
omega_dec=0.052*omega_jan;


sim asynchronous_gen_backupgio_hines_thesis;     %connect input torque
load data3;
delay_time=-.0045-.0005;

%load data3;
%------------------------------------------------------------------------
%Plots


figure(1);  %Speed plot measured and simulated
plot(timedataold',ch8_final,'b','linewidth',2);
hold on;
plot(speed_sim(:,1)-30,speed_sim(:,2),'g','linewidth',2)
hold off;
axis([0 30 1400 2000]);
%title('Measured and Simulated Speed');
legend('RPM Measured','RPM Simulated', 'Location', 'NorthWest');
ylabel('Machine Speed (RPM)');
xlabel('Time(Seconds)');
grid;

figure(2);  % Input Power plot measured and simulated
plot(ScopeData14(:,1)-30,ScopeData14(:,2),'g','linewidth',2);
```

```matlab
hold on;
plot(time_dc,dc_machine_power,'b','linewidth',2);
hold off;
axis ([0 30 110 220]);
%title('Rotor Input Power of DC Motor');
legend('Simulated Input Power', 'Measured Input Power',
'Location','NorthWest');
ylabel('Input Power (Watts)');
xlabel('Time (Seconds)');
grid;


%----------------------------------------------------------------
----
%Connect the monthly summation block in the induction machine model

figure(3);                              %Monthly speed figure
plot(speed_sim(:,1)-30,speed_sim(:,2),'g','linewidth',2)
axis([0 48 1300 1900]);
%title('Simulated Average DC Motor Speed Scaled by Monthly Norfolk Wind
Speeds');
legend('RPM_{O} For Simulated Wind Speed', 'Location', 'NorthEast');
ylabel('Machine Speed (RPM)');
xlabel('Time(Seconds)');
grid;


figure(4); %Monthly Power Figure
plot(power_out(:,1)-30,power_out(:,2),'g','linewidth',2);
axis ([0 48 110 180]);
%title('Simulated Mechanical Output Power of DC Motor Scaled by Monthly
Norfolk Winds Speeds');
legend('Output Power by Month for Norfolk', 'Location','NorthEast');
ylabel('Output Power (Watts)');
xlabel('Time (Seconds)');
grid;
%----------------------------------------------------------------
----
plot_exp_data_newscope;

figure(5);  %Armature and Field Currents
plot(ia_plot(:,1)-30,ia_plot(:,2), 'g', 'linewidth',4); %Simulated Ia
hold on;
plot(datavec_ch4(:,1)+13.8,ch4_smooth,'b'); %Measured Armature Current
plot(if_plot(:,1)-30, if_plot(:,2), 'c', 'linewidth',4); %Simulated If
plot(datavec(:,1)+13.8,ch2_smooth,'m'); %Measured Field Current
hold off;
axis([12.5 15 0.2 1.4]);
%title('Simulated and Measured Armature and Field Currents');
legend('Simulated Armature Current', 'Measured Armature
Current','Simulated Field Current', 'Measured Field Current',
'Location', 'East');
ylabel('Current (Amperes)');
xlabel('Time (Seconds)');
grid;
```

```matlab
figure(6);   %Output Power plot
plot(power_out(:,1)-30,power_out(:,2),'g','linewidth',2);
axis ([0 30 110 200]);
%title('Simulated Mechanical Output Power of DC Motor');
legend('Simulated Output Power', 'Location','NorthWest');
ylabel('Output Power (Watts)');
xlabel('Time (Seconds)');
grid;


figure(7);   %Speed plot measured
plot(timedataold',ch8_final,'b','linewidth',2);
axis([0 30 1400 2000]);
%title('Measured Speed');
legend('RPM Measured', 'Location', 'NorthWest');
ylabel('Machine Speed (RPM)');
xlabel('Time(Seconds)');
grid;


figure(8);   %Speed plot simulated
plot(speed_sim(:,1)-30,speed_sim(:,2),'g','linewidth',2)
axis([0 30 1400 2000]);
%title('Simulated Speed');
legend('RPM Simulated', 'Location', 'NorthWest');
ylabel('Machine Speed (RPM)');
xlabel('Time(Seconds)');
grid;


figure(9);   % Input Power plot Simulated
plot(ScopeData14(:,1)-30,ScopeData14(:,2),'g','linewidth',2);
axis ([0 30 110 220]);
%title('Simulated Rotor Input Power of DC Motor');
legend('Simulated Input Power', 'Location', 'NorthWest');
ylabel('Input Power (Watts)');
xlabel('Time (Seconds)');
grid;


figure(10);   % Input Power plot Measured
plot(time_dc,dc_machine_power,'b','linewidth',2);
axis ([0 30 110 220]);
%title('Measured Rotor Input Power of DC Motor');
legend('Measured Input Power', 'Location', 'NorthWest');
ylabel('Input Power (Watts)');
xlabel('Time (Seconds)');
grid;
```

**initial_vars_asynchronous_gen.m, from [3]**

```matlab
%initial_vars_asynchronous_gen

omega_b = 2*pi*60;
% omega2=-omega_b*1/14;
tstep=.0008;
tstop=60;
twopiby3 = 2*pi/3;
poles = 4;
polesby2J = poles/2/(2.04e-3*1.5); %Inertia from Nytko thesis
Kpgain_speed=.033*2;
Kigain_speed=.0033*4;
Kpgain=15/2*10;      % Divide by 2 becuae Vdc=60 is half of 120 in the
FPGA program
Kigain=2/2*40;
%Parameters from Edwards thesis work for DFIG
rs=12;
rr = 4;
Xls =9;
Xm =180*0.6;     % no load
Xm =180*0.7;     % with generation
Xlr = 9+omega_b*400e-6;

rsbyXls = rs/Xls;
rrbyXlr = rr/Xlr;
Xaq = 1/(1/Xm+1/Xls+1/Xlr);
Xad = Xaq;
XaqbyXls = Xaq/Xls;
XaqbyXlr = Xaq/Xlr;
XadbyXls = Xad/Xls;
XadbyXlr = Xad/Xlr;
V_phase = 220*sqrt(2)/sqrt(3);  %Peak value used in Simulink for source
model

% omegar_ic = omega_b*13/14;
psi_qsic=0;
psi_dsic=0;
psi_qric=0;
psi_dric=0;
```

**shift_time2.m from [3]**

```matlab
%shift_time2

function [data]= shift_time2 (z15_LSB, z15_MSB, z16_LSB, z16_MSB,
data_size)

    z15_new_LSB=uint8(zeros(data_size,1));
    z15_new_MSB=uint8(zeros(data_size,1));
    index=0;
    for ii=1:data_size
        if z15_MSB(ii)>=2^7
        index=index+1;
            z15_new_MSB(ii)=z15_MSB(ii)-2^7;
            if z15_new_MSB(ii)>=2^6
        index=index+1;
                z15_new_MSB(ii)=z15_new_MSB(ii)-2^6;
            end
        elseif z15_MSB(ii)>=2^6
                z15_new_MSB(ii)=z15_MSB(ii)-2^6;
        else
        z15_new_MSB(ii)=z15_MSB(ii);
        end
    end
    index=0;
    for ii=1:data_size
        if z15_LSB(ii)>=2^7
        index=index+1;
            z15_new_LSB(ii)=z15_LSB(ii)-2^7;
            if z15_new_LSB(ii)>=2^6
        index=index+1;
                z15_new_LSB(ii)=z15_new_LSB(ii)-2^6;
            end
        elseif z15_LSB(ii)>=2^6
                z15_new_LSB(ii)=z15_LSB(ii)-2^6;
        else
        z15_new_LSB(ii)=z15_LSB(ii);
        end
    end
    %channel 16
    z16_new_LSB=uint8(zeros(data_size,1));
    z16_new_MSB=uint8(zeros(data_size,1));
    index=0;
    for ii=1:data_size
        if z16_MSB(ii)>=2^7
        index=index+1;
            z16_new_MSB(ii)=z16_MSB(ii)-2^7;
            if z16_new_MSB(ii)>=2^6
        index=index+1;
                z16_new_MSB(ii)=z16_new_MSB(ii)-2^6;
            end
        elseif z16_MSB(ii)>=2^6
                z16_new_MSB(ii)=z16_MSB(ii)-2^6;
        else
```

55

```matlab
        z16_new_MSB(ii)=z16_MSB(ii);
        end
    end
    index=0;
    for ii=1:data_size
        if z16_LSB(ii)>=2^7
        index=index+1;
            z16_new_LSB(ii)=z16_LSB(ii)-2^7;
            if z16_new_LSB(ii)>=2^6
        index=index+1;
                z16_new_LSB(ii)=z16_new_LSB(ii)-2^6;
            end
        elseif z16_LSB(ii)>=2^6
                z16_new_LSB(ii)=z16_LSB(ii)-2^6;
        else
        z16_new_LSB(ii)=z16_LSB(ii);
        end
    end
data15=(double(z15_new_LSB)+double(z15_new_MSB)*2^6);
data16=(double(z16_new_LSB)+double(z16_new_MSB)*2^6)*2^12;
data=((data15+data16)-(data15(1)+data16(1)))*2^17/25e6;
```

## shift2alj.m, from [3]

```matlab
%shift2alj

function [data]= shiftb2 (z_LSB, z_MSB,data_size)


    z_new_LSB=uint8(zeros(data_size,1));
    z_new_MSB=uint8(zeros(data_size,1));
    index=0;
    for ii=1:data_size
        if z_MSB(ii)>=2^7
        index=index+1;
            z_new_MSB(ii)=z_MSB(ii)-2^7;
            if z_new_MSB(ii)>=2^6
        index=index+1;
                z_new_MSB(ii)=z_new_MSB(ii)-2^6;
            end
        elseif z_MSB(ii)>=2^6
                z_new_MSB(ii)=z_MSB(ii)-2^6;
        else
        z_new_MSB(ii)=z_MSB(ii);
        end
    end
    index=0;
    for ii=1:data_size
        if z_LSB(ii)>=2^7
        index=index+1;
            z_new_LSB(ii)=z_LSB(ii)-2^7;
            if z_new_LSB(ii)>=2^6
        index=index+1;
                z_new_LSB(ii)=z_new_LSB(ii)-2^6;
            end
        elseif z_LSB(ii)>=2^6
                z_new_LSB(ii)=z_LSB(ii)-2^6;
        else
        z_new_LSB(ii)=z_LSB(ii);
        end
    end
    for ii=1:data_size
        if z_new_MSB(ii) >= 2^5
            data(ii)=(double(z_new_LSB(ii))+double(z_new_MSB(ii))*2^6-
double(2^12));
        else
            data(ii)=(double(z_new_LSB(ii))+double(z_new_MSB(ii))*2^6);
        end
    end
```

**plot_exp_data_newscope.m, from [3]**

```matlab
% EC3150 – Laboratory – G.Oriti, Jul '09
% This file acquires the data vector from the oscilloscope
% and plots it versus time
% It also plots the spectrum of the input data vector using the fft

data_in=xlsread('Tek_CH2_Wfm.csv');
data_in_ch3=xlsread('Tek_CH3_Wfm.csv');
data_in_ch4=xlsread('Tek_CH4_Wfm.csv');
len = length(data_in);
datavec=data_in(15:len,1:2);
datavec_ch3=data_in_ch3(15:len,1:2);
datavec_ch4=data_in_ch4(15:len,1:2);


ch2_smooth=(datavec(:,2)+[datavec(2:len-14,2);0])/2;
ch3_smooth=(datavec_ch3(:,2)+[datavec_ch3(2:len-14,2);0])/2;
ch4_smooth=(datavec_ch4(:,2)+[datavec_ch4(2:len-14,2);0])/2;
figure(1);
% plot(datavec(:,1),datavec(:,2),'b:');
plot(datavec(:,1),ch2_smooth,'m');
hold on;
% plot(datavec_ch3(:,1),datavec_ch3(:,2)/10-15,'g');
% plot(datavec_ch4(:,1),datavec_ch4(:,2),'r');
%plot(datavec_ch3(:,1),ch3_smooth/10-15,'k');
plot(datavec_ch4(:,1),ch4_smooth,'b');
hold off;
title('DC Machine measurements during step change in speed');
xlabel('time [s]');
grid on
legend('I_f_i_e_l_d','I_a','Location','NorthEast');
axis([-1 1 0 4]);
```

**Data_crunching.m from [3]**

```
%data_crunching


%post-processing and plotting data
%processing channel 1 data
z_LSB1a=z(:,1);
z_MSB1a=z(:,2);
z_LSB1b=z(:,1+32);
z_MSB1b=z(:,2+32);
z_LSB1c=z(:,1+32+32);
z_MSB1c=z(:,2+32+32);
z_LSB1d=z(:,1+32+32+32);
z_MSB1d=z(:,2+32+32+32);
z_LSB1e=z(:,1+16);
z_MSB1e=z(:,2+16);
z_LSB1f=z(:,1+32+16);
z_MSB1f=z(:,2+32+16);
z_LSB1g=z(:,1+32+32+16);
z_MSB1g=z(:,2+32+32+16);
z_LSB1h=z(:,1+32+32+32+16);
z_MSB1h=z(:,2+32+32+32+16);

for ii=1:totalpoints/2
    z_LSB1(8*ii-7)  =z_LSB1a(ii);
    z_LSB1(8*ii-6)  =z_LSB1e(ii);
    z_LSB1(8*ii-5)  =z_LSB1b(ii);
    z_LSB1(8*ii-4)  =z_LSB1f(ii);
    z_LSB1(8*ii-3)  =z_LSB1c(ii);
    z_LSB1(8*ii-2)  =z_LSB1g(ii);
    z_LSB1(8*ii-1)  =z_LSB1d(ii);
    z_LSB1(8*ii)    =z_LSB1h(ii);
    z_MSB1(8*ii-7)  =z_MSB1a(ii);
    z_MSB1(8*ii-6)  =z_MSB1e(ii);
    z_MSB1(8*ii-5)  =z_MSB1b(ii);
    z_MSB1(8*ii-4)  =z_MSB1f(ii);
    z_MSB1(8*ii-3)  =z_MSB1c(ii);
    z_MSB1(8*ii-2)  =z_MSB1g(ii);
    z_MSB1(8*ii-1)  =z_MSB1d(ii);
    z_MSB1(8*ii)    =z_MSB1h(ii);
end

ch1_data= shiftb2alj (z_LSB1, z_MSB1, totalpoints*4);
ch1_final=ch1_data/2^2;

%processing channel 4 data
gain1=1/(1/3000+1/200000)/(1/(1/3000+1/200000)+56000*2)*1.05;
z_LSB4a=z(:,7);
z_MSB4a=z(:,8);
z_LSB4b=z(:,7+32);
z_MSB4b=z(:,8+32);
z_LSB4c=z(:,7+32+32);
z_MSB4c=z(:,8+32+32);
```

```matlab
z_LSB4d=z(:,7+32+32+32);
z_MSB4d=z(:,8+32+32+32);
z_LSB4e=z(:,7+16);
z_MSB4e=z(:,8+16);
z_LSB4f=z(:,7+32+16);
z_MSB4f=z(:,8+32+16);
z_LSB4g=z(:,7+32+32+16);
z_MSB4g=z(:,8+32+32+16);
z_LSB4h=z(:,7+32+32+32+16);
z_MSB4h=z(:,8+32+32+32+16);


for ii=1:totalpoints/2
    z_LSB4(8*ii-7)  =z_LSB4a(ii);
    z_LSB4(8*ii-6)  =z_LSB4e(ii);
    z_LSB4(8*ii-5)  =z_LSB4b(ii);
    z_LSB4(8*ii-4)  =z_LSB4f(ii);
    z_LSB4(8*ii-3)  =z_LSB4c(ii);
    z_LSB4(8*ii-2)  =z_LSB4g(ii);
    z_LSB4(8*ii-1)  =z_LSB4d(ii);
    z_LSB4(8*ii)    =z_LSB4h(ii);
    z_MSB4(8*ii-7)  =z_MSB4a(ii);
    z_MSB4(8*ii-6)  =z_MSB4e(ii);
    z_MSB4(8*ii-5)  =z_MSB4b(ii);
    z_MSB4(8*ii-4)  =z_MSB4f(ii);
    z_MSB4(8*ii-3)  =z_MSB4c(ii);
    z_MSB4(8*ii-2)  =z_MSB4g(ii);
    z_MSB4(8*ii-1)  =z_MSB4d(ii);
    z_MSB4(8*ii)    =z_MSB4h(ii);
end

ch4_data= shiftb2alj (z_LSB4, z_MSB4, totalpoints*4);
ch4_final=ch4_data/2^2;
%processing channel 5 data
z_LSB5a=z(:,9);
z_MSB5a=z(:,10);
z_LSB5b=z(:,9+32);
z_MSB5b=z(:,10+32);
z_LSB5c=z(:,9+32+32);
z_MSB5c=z(:,10+32+32);
z_LSB5d=z(:,9+32+32+32);
z_MSB5d=z(:,10+32+32+32);
z_LSB5e=z(:,9+16);
z_MSB5e=z(:,10+16);
z_LSB5f=z(:,9+32+16);
z_MSB5f=z(:,10+32+16);
z_LSB5g=z(:,9+32+32+16);
z_MSB5g=z(:,10+32+32+16);
z_LSB5h=z(:,9+32+32+32+16);
z_MSB5h=z(:,10+32+32+32+16);


for ii=1:totalpoints/2
    z_LSB5(8*ii-7)  =z_LSB5a(ii);
    z_LSB5(8*ii-6)  =z_LSB5e(ii);
    z_LSB5(8*ii-5)  =z_LSB5b(ii);
    z_LSB5(8*ii-4)  =z_LSB5f(ii);
```

```
        z_LSB5(8*ii-3)  =z_LSB5c(ii);
        z_LSB5(8*ii-2)  =z_LSB5g(ii);
        z_LSB5(8*ii-1)  =z_LSB5d(ii);
        z_LSB5(8*ii)    =z_LSB5h(ii);
        z_MSB5(8*ii-7)  =z_MSB5a(ii);
        z_MSB5(8*ii-6)  =z_MSB5e(ii);
        z_MSB5(8*ii-5)  =z_MSB5b(ii);
        z_MSB5(8*ii-4)  =z_MSB5f(ii);
        z_MSB5(8*ii-3)  =z_MSB5c(ii);
        z_MSB5(8*ii-2)  =z_MSB5g(ii);
        z_MSB5(8*ii-1)  =z_MSB5d(ii);
        z_MSB5(8*ii)    =z_MSB5h(ii);
    end
    ch5_data= shiftb2alj (z_LSB5, z_MSB5, totalpoints*4);
    ch5_final=ch5_data/2^2;
    %processing channel 6 data
    gain2=1/(1/6800+1/200000)/(1/(1/6800+1/200000)+120000*2)*1.05;  %DC
    sensor gain
    gainI=3/1000*330;              %current sensor gain
    z_LSB6a=z(:,11);
    z_MSB6a=z(:,12);
    z_LSB6b=z(:,11+32);
    z_MSB6b=z(:,12+32);
    z_LSB6c=z(:,11+32+32);
    z_MSB6c=z(:,12+32+32);
    z_LSB6d=z(:,11+32+32+32);
    z_MSB6d=z(:,12+32+32+32);
    z_LSB6e=z(:,11+16);
    z_MSB6e=z(:,12+16);
    z_LSB6f=z(:,11+32+16);
    z_MSB6f=z(:,12+32+16);
    z_LSB6g=z(:,11+32+32+16);
    z_MSB6g=z(:,12+32+32+16);
    z_LSB6h=z(:,11+32+32+32+16);
    z_MSB6h=z(:,12+32+32+32+16);

    for ii=1:totalpoints/2
        z_LSB6(8*ii-7)  =z_LSB6a(ii);
        z_LSB6(8*ii-6)  =z_LSB6e(ii);
        z_LSB6(8*ii-5)  =z_LSB6b(ii);
        z_LSB6(8*ii-4)  =z_LSB6f(ii);
        z_LSB6(8*ii-3)  =z_LSB6c(ii);
        z_LSB6(8*ii-2)  =z_LSB6g(ii);
        z_LSB6(8*ii-1)  =z_LSB6d(ii);
        z_LSB6(8*ii)    =z_LSB6h(ii);
        z_MSB6(8*ii-7)  =z_MSB6a(ii);
        z_MSB6(8*ii-6)  =z_MSB6e(ii);
        z_MSB6(8*ii-5)  =z_MSB6b(ii);
        z_MSB6(8*ii-4)  =z_MSB6f(ii);
        z_MSB6(8*ii-3)  =z_MSB6c(ii);
        z_MSB6(8*ii-2)  =z_MSB6g(ii);
        z_MSB6(8*ii-1)  =z_MSB6d(ii);
        z_MSB6(8*ii)    =z_MSB6h(ii);
    end
    ch6_data= shiftb2alj (z_LSB6, z_MSB6, totalpoints*4);
```

```matlab
ch6_final=ch6_data/2^6;
%processing channel 7 data
z_LSB7a=z(:,13);
z_MSB7a=z(:,14);
z_LSB7b=z(:,13+32);
z_MSB7b=z(:,14+32);
z_LSB7c=z(:,13+32+32);
z_MSB7c=z(:,14+32+32);
z_LSB7d=z(:,13+32+32+32);
z_MSB7d=z(:,14+32+32+32);
z_LSB7e=z(:,13+16);
z_MSB7e=z(:,14+16);
z_LSB7f=z(:,13+32+16);
z_MSB7f=z(:,14+32+16);
z_LSB7g=z(:,13+32+32+16);
z_MSB7g=z(:,14+32+32+16);
z_LSB7h=z(:,13+32+32+32+16);
z_MSB7h=z(:,14+32+32+32+16);


for ii=1:totalpoints/2
    z_LSB7(8*ii-7)  =z_LSB7a(ii);
    z_LSB7(8*ii-6)  =z_LSB7e(ii);
    z_LSB7(8*ii-5)  =z_LSB7b(ii);
    z_LSB7(8*ii-4)  =z_LSB7f(ii);
    z_LSB7(8*ii-3)  =z_LSB7c(ii);
    z_LSB7(8*ii-2)  =z_LSB7g(ii);
    z_LSB7(8*ii-1)  =z_LSB7d(ii);
    z_LSB7(8*ii)    =z_LSB7h(ii);
    z_MSB7(8*ii-7)  =z_MSB7a(ii);
    z_MSB7(8*ii-6)  =z_MSB7e(ii);
    z_MSB7(8*ii-5)  =z_MSB7b(ii);
    z_MSB7(8*ii-4)  =z_MSB7f(ii);
    z_MSB7(8*ii-3)  =z_MSB7c(ii);
    z_MSB7(8*ii-2)  =z_MSB7g(ii);
    z_MSB7(8*ii-1)  =z_MSB7d(ii);
    z_MSB7(8*ii)    =z_MSB7h(ii);
end
ch7_data= shiftb2alj (z_LSB7, z_MSB7, totalpoints*4);
ch7_final=ch7_data/2^6;


%processing channel 8 data
z_LSB8a=z(:,15);
z_MSB8a=z(:,16);
z_LSB8b=z(:,15+32);
z_MSB8b=z(:,16+32);
z_LSB8c=z(:,15+32+32);
z_MSB8c=z(:,16+32+32);
z_LSB8d=z(:,15+32+32+32);
z_MSB8d=z(:,16+32+32+32);
z_LSB8e=z(:,15+16);
z_MSB8e=z(:,16+16);
z_LSB8f=z(:,15+32+16);
z_MSB8f=z(:,16+32+16);
z_LSB8g=z(:,15+32+32+16);
z_MSB8g=z(:,16+32+32+16);
```

```matlab
z_LSB8h=z(:,15+32+32+32+16);
z_MSB8h=z(:,16+32+32+32+16);

for ii=1:totalpoints/2
    z_LSB8(8*ii-7)  =z_LSB8a(ii);
    z_LSB8(8*ii-6)  =z_LSB8e(ii);
    z_LSB8(8*ii-5)  =z_LSB8b(ii);
    z_LSB8(8*ii-4)  =z_LSB8f(ii);
    z_LSB8(8*ii-3)  =z_LSB8c(ii);
    z_LSB8(8*ii-2)  =z_LSB8g(ii);
    z_LSB8(8*ii-1)  =z_LSB8d(ii);
    z_LSB8(8*ii)    =z_LSB8h(ii);
    z_MSB8(8*ii-7)  =z_MSB8a(ii);
    z_MSB8(8*ii-6)  =z_MSB8e(ii);
    z_MSB8(8*ii-5)  =z_MSB8b(ii);
    z_MSB8(8*ii-4)  =z_MSB8f(ii);
    z_MSB8(8*ii-3)  =z_MSB8c(ii);
    z_MSB8(8*ii-2)  =z_MSB8g(ii);
    z_MSB8(8*ii-1)  =z_MSB8d(ii);
    z_MSB8(8*ii)    =z_MSB8h(ii);
end
ch8_data= shiftb2alj (z_LSB8, z_MSB8, totalpoints*4);
ch8_final=ch8_data;

%processing channel 2 and 3 data to create time vector

%processing channel 2 data
z_LSB2a=z(:,3);
z_MSB2a=z(:,4);
z_LSB2b=z(:,3+32);
z_MSB2b=z(:,4+32);
z_LSB2c=z(:,3+32+32);
z_MSB2c=z(:,4+32+32);
z_LSB2d=z(:,3+32+32+32);
z_MSB2d=z(:,4+32+32+32);
z_LSB2e=z(:,3+16);
z_MSB2e=z(:,4+16);
z_LSB2f=z(:,3+32+16);
z_MSB2f=z(:,4+32+16);
z_LSB2g=z(:,3+32+32+16);
z_MSB2g=z(:,4+32+32+16);
z_LSB2h=z(:,3+32+32+32+16);
z_MSB2h=z(:,4+32+32+32+16);

for ii=1:totalpoints/2
    z_LSB2(8*ii-7)  =z_LSB2a(ii);
    z_LSB2(8*ii-6)  =z_LSB2e(ii);
    z_LSB2(8*ii-5)  =z_LSB2b(ii);
    z_LSB2(8*ii-4)  =z_LSB2f(ii);
    z_LSB2(8*ii-3)  =z_LSB2c(ii);
    z_LSB2(8*ii-2)  =z_LSB2g(ii);
    z_LSB2(8*ii-1)  =z_LSB2d(ii);
    z_LSB2(8*ii)    =z_LSB2h(ii);
    z_MSB2(8*ii-7)  =z_MSB2a(ii);
    z_MSB2(8*ii-6)  =z_MSB2e(ii);
```

```matlab
    z_MSB2(8*ii-5)  =z_MSB2b(ii);
    z_MSB2(8*ii-4)  =z_MSB2f(ii);
    z_MSB2(8*ii-3)  =z_MSB2c(ii);
    z_MSB2(8*ii-2)  =z_MSB2g(ii);
    z_MSB2(8*ii-1)  =z_MSB2d(ii);
    z_MSB2(8*ii)    =z_MSB2h(ii);
end
%processing channel 3 data
z_LSB3a=z(:,5);
z_MSB3a=z(:,6);
z_LSB3b=z(:,5+32);
z_MSB3b=z(:,6+32);
z_LSB3c=z(:,5+32+32);
z_MSB3c=z(:,6+32+32);
z_LSB3d=z(:,5+32+32+32);
z_MSB3d=z(:,6+32+32+32);
z_LSB3e=z(:,5+16);
z_MSB3e=z(:,6+16);
z_LSB3f=z(:,5+32+16);
z_MSB3f=z(:,6+32+16);
z_LSB3g=z(:,5+32+32+16);
z_MSB3g=z(:,6+32+32+16);
z_LSB3h=z(:,5+32+32+32+16);
z_MSB3h=z(:,6+32+32+32+16);

for ii=1:totalpoints/2
    z_LSB3(8*ii-7)  =z_LSB3a(ii);
    z_LSB3(8*ii-6)  =z_LSB3e(ii);
    z_LSB3(8*ii-5)  =z_LSB3b(ii);
    z_LSB3(8*ii-4)  =z_LSB3f(ii);
    z_LSB3(8*ii-3)  =z_LSB3c(ii);
    z_LSB3(8*ii-2)  =z_LSB3g(ii);
    z_LSB3(8*ii-1)  =z_LSB3d(ii);
    z_LSB3(8*ii)    =z_LSB3h(ii);
    z_MSB3(8*ii-7)  =z_MSB3a(ii);
    z_MSB3(8*ii-6)  =z_MSB3e(ii);
    z_MSB3(8*ii-5)  =z_MSB3b(ii);
    z_MSB3(8*ii-4)  =z_MSB3f(ii);
    z_MSB3(8*ii-3)  =z_MSB3c(ii);
    z_MSB3(8*ii-2)  =z_MSB3g(ii);
    z_MSB3(8*ii-1)  =z_MSB3d(ii);
    z_MSB3(8*ii)    =z_MSB3h(ii);
end

timedataold= shift_time2 (z_LSB2, z_MSB2, z_LSB3, z_MSB3,
totalpoints*4);

    timedata=[0:(2^11-1)]/25e6*2^12;
```

# LIST OF REFERENCES

[1]     "Defense infrastructure: Department of Defense renewable energy initiatives," Briefing for the Committees on Armed Services, United States Senate and House of Representatives. Government Accountability Office, 26 April 2010.

[2]     S. Muller, M. Deicke, and R. W. de Doncker. "Doubly fed induction generator systems for wind turbines." *IEEE Industry Applications Magazine*, pp. 26–33, May/June 2002.

[3]     A. L. Julian and G. Oriti. Class notes for EC4130, Advanced Electrical Machinery Systems and Work on DFIG, Naval Postgraduate School, 2007–2012 (unpublished).

[4]     J. R. Derges, "Torque control of a separate-winding excitation DC motor for a dynamometer," M.S. thesis, Naval Postgraduate School, 2010.

[5]     P. C. Krause, O. Wasynczuk, and S. D. Sudhoff, *Analysis of Electric Machinery and Drive Systems*. Hoboken, NJ: John Wiley & Sons, 2002.

[6]     Dan Dellinger. "Wind- average wind speed- (MPH), " August 20, 2008 [Online]. Available: http://lwf.ncdc.noaa.gov/oa/climate/online/ccd/avgwind.html

THIS PAGE INTENTIONALLY LEFT BLANK

# INITIAL DISTRIBUTION LIST

1.  Defense Technical Information Center
    Ft. Belvoir, Virginia

2.  Dudley Knox Library
    Naval Postgraduate School
    Monterey, California

3.  Dr. R. Clark Robertson
    Navy Postgraduate School
    Monterey, California

4.  Dr. Alexander L. Julian
    Navy Postgraduate School
    Monterey, California

5.  Dr. Giovanna Oriti
    Navy Postgraduate School
    Monterey, California

6.  LT Jonathan T. Hines, USN
    NAVSUBSCOL New London
    Groton, Connecticut